DIPLOMARBEIT

SLOWLY PULSATING B STARS DISCOVERED EMPLOYING MOST GUIDE STAR PHOTOMETRY

angestrebter akademischer Grad
Magister der Naturwissenschaften (Mag. rer. nat.)

Verfasser: David Gruber Bakk. rer. nat.

Matrikel-Nummer: 0303287

Studienrichtung: A 066 861

Betreuer: Ao. Univ.-Prof. tit. Univ.-Prof. Dipl.-Ing. Dr. Werner Wolfgang Weiss

Wien, im Mai 2009

Für meine Eltern

Contents

Abstract

MOST, the first Canadian space telescope (launched in June 2003), has been designed primarily to perform high-precision photometry of bright stars ($V < 6^{\mathrm{m}}$) nearly continuously over long time spans of up to 60 days. In the last five years, the capabilities of MOST have been extended and enhanced to allow photometry of stars as faint as $V \sim 13^{\mathrm{m}}$. MOST has monitored more than 1000 stars, most of which are guide stars in the fields containing Primary Science Targets. Many variable stars have been discovered in this large guide star sample, spread across the HR Diagram, including more than 23 SPB (Slowly Pulsating B) stars. For this class of stars, MOST offers unprecedented time coverage, precision and frequency resolution. Data and frequency analysis of the SPB stars discovered by MOST are presented and discussed here.

MOST, das erste kanadische Weltraumteleskop wurde im Juni 2003 in die Erdumlaufbahn befördert. Die Aufgabe dieses Satelliten war und ist es nach wie vor, ununterbrochene, hochpräzise Photometrie von hellen Sternen ($V < 6^{\mathrm{m}}$) über einen sehr langen Zeitraum durchzuführen. In den letzten fünf Jahren konnten die Möglichkeiten von MOST ausgebaut und verbessert werden und MOST kann inzwischen Sterne mit einer scheinbaren Helligkeit von $V \sim 13^{\mathrm{m}}$ messen. MOST hat über 1000 Sterne photometriert; Die meisten davon sind Leitsterne in den Feldern, in denen sich die primären wissenschaftlichen Beobachtungsobjekte befinden. Viele von diesen Leitsternen, die sich quer über das Hertzsprung-Russel Diagramm ausbreiten, konnten bereits als variabel klassifiziert werden. 23 der Letztgenannten sind so genannte ,,slowly pulsating B stars" (langsam pulsierende B Sterne), für welche MOST eine bis dato unerreichte Präzision und Frequenzauflösung erreicht hat. Im Folgenden werden die Daten und die Frequenzanalyse der von MOST entdeckten SPB Sterne dargestellt.

Preface

> Stars scribble in our eyes the frosty sagas, the gleaming cantos of unvanquished space.
> - Hart Crane

When one looks up and gazes at the nightly sky one can see countless stars which glitter all over the skies. By doing this, our earliest ancestors gave birth to the oldest science of mankind: astronomy. Since then, new discoveries have been and are still made to this day. One of the major discoveries was the detection of stellar variability, caused by occultations from companion stars or even more importantly for astrophysics, by intrinsic effects, i.e. stellar pulsations. The genius idea was to observe this variability in the most accurate way to investigate the internal structure and thus to understand the evolution of a star (comparable to the work of seismologists who use earthquake waves to determine the internal structure of the Earth). This fairly new astronomic branch, which has established itself to a major research field, is called "asteroseismology"

Due to the hampering effects of our atmosphere and the observing gaps in the data sets caused by the day to night changes, Earth-based observations are very challenging and demanding even today. The "greedy" need for new and better data forced astronomers to observe from space with satellites.

In June 2003, the canadian microsatellite "Microvariability and Oscillation of STars" (MOST) was launched into an 800 km orbit. MOST's only goal was (and still is) to support asteroseismological research; i.e. to perform high-precision photometry from space. In spite of MOST's small size and an instrument comparable to an amateur telescope, the satellite is in its fifth year in space, it still delivers data at outstanding quality and precision, and it had a great impact into the astronomic community. Even the guide star photometry, which was designed exclusively for the attitude control system, outperforms ground based data in many cases by far.

One of the many different classes of variable stars which are observed by the MOST satellite are the so-called SPB (slowly pulsating B) stars (see Chapter 2). MOST detected more than 20 new candidates of this class in the past five years which are subject of this master thesis.

The present work is divided into 7 chapters. In Chapter 1, the reader is introduced in the MOST project with its goals, the instrument and the working methods. Chapter 2 deals with properties of SPB stars, Chapter 3 describes the stellar modelling process, Chapter 4 provides an introduction to frequency analysis and the various software tools employed, Chapter 5 and 6 present the investigated stars and the main scientific results and Chapter 7, finally, sums up the work of this master thesis.

Chapter 1

The MOST Space Telescope

1.1 Why observe from space?

One may ask why we literally spend millions and billions of dollars to observe from an in itself hostile space, if we already have so many well-performing telescopes, e.g. the VLT (Very Large Telescope) in Chile, on our familiar and beloved Earth. There are mainly two reasons:

1. regular observing gaps, e.g. the unavoidable day to night variations produce so called aliasing effects in the spectral window. These peaks can be misinterpreted as intrinsic stellar signal and thus lead to wrong interpretation of the data set.
2. Earth's atmosphere, so crucial for mankind, is the astronomer's nightmare. Molecules (Rayleigh scattering), dust and aerosols absorb and scatter incoming radiation. Another annoying effect of the atmosphere is refraction. In combination with temperature and pressure variations, refraction causes a rapid change in size, position and apparent brightness of the observed star. These effects, which are more significant for point sources (such as stars) are called "seeing" and "scintillation", respectively. Especially scintillation, for a layman the romantic glittering of a star, is terrible for asteroseismologists because it causes major intensity variations (up to one magnitude for stars in the vicinity of the horizon) which are not inherent to the star.

Nowadays noise in the data can be diminished by very sophisticated and complex mechanisms, e.g. multi-site campaigns (such as the Whole Earth Telescope) which require a great effort, or active and adaptive optics (used by the Very Large Telescope). But to increase our understanding of stellar oscillations and thus to get down to accuracies of parts-per-million (ppm), space observatories are inevitable.

1.2 What is MOST?

The "Microvariability and Oscillation of STars" or "Microvariabilité et Oscillations STellaires" (MOST)[1] mission (fully described in Walker et al. (2003)) is Canada's first space satellite launched

[1]MOST is part of the CSA Small Payloads Program with additional funding provided by the Ontario Research and Development Challenge Fund, the Natural Sciences and Engineering Research Council (NSERC), the Ontario Centre for Research in Earth and Space Technology, and the Universities of Toronto, British Columbia, and Vienna.

on June 30, 2003. The primary goal of this microsatellite is to detect photometric oscillations of solar-type stars; but also reflected light from giant exoplanets, roAp stars (Gruberbauer et al. 2008); (Huber et al. 2008) and Wolf-Rayet stars (Moffat et al. 2008) are included in the MOST target selection. The costs of this space mission are low compared to similar space projects with similar scientific goals. This is certainly due to the fact that MOST is a relatively small ($65\times65\times30$ cm) and light satellite (54kg). However, the time coverage and precision of the photometry is unachievable from ground even with observatory networks. Usually satellites carrying optical telescopes are large. This is simply due to the fact that the stability of a satellite depends on its inertia to give the attitude control system (ACS)[2] enough time for the adjustment of drifts. The best pointing accuracy of satellites before MOST was about $\pm2^\circ$. Only a new Canadian technology made it possible to develop a new attitude control system which was able to perform better by two orders of magnitude.

1.3 Basic design

MOST's design is optimized to achieve micromagnitude precision for the stellar amplitude spectrum in the 2000-4000 μHz domain for stars with magnitudes from $0.4^{\rm m}$ and $5.5^{\rm m}$. MOST sources its energy from solar panels which provide a power supply of 30 W, of which only 10 W (provided mainly by the backside solar panels) are effectively available to the instrument. The additional solar panels on the front side of the spacecraft were only used to gain additional power to stabilize the satellite after its release from the rocket. The spacecraft is stabilized by three sets of reaction wheels and magnetotorquers which give MOST an exceptional pointing accuracy never reached by a microsatellite before. Originally an accuracy of ±25 arcsec was required for pointing, but MOST is now down to ±1 arcsec. The only flexible part on the spacecraft is a motorized shutter which is used to close the entrance aperture, if the satellite is endangered to stare towards the Sun to prevent a detector meltdown.

1.4 Instrument

The telescope is the core part of the mission. It is a 150 mm aperture Rumak-Maksutov made of Invar, with a focal ratio of f/6 fed by a 45° periscope mirror due to the limited width of the housing (see Fig.1.2). The mirrors are made of fused silica allowing an operation without active focusing since this material allows athermal performance. Schott BK7 glass is used for both the field corrector and CCD window to absorb UV radiation from cosmic ray Cherencok flashes in the fused silica corrector lens of the telescope. The field of view is 1.28° with an unvignetted field of 0.4°. The telescope is shielded from the Sun which in turn can illuminate the solar cells on the backside. The entering light is focused on the guidance and science CCDs at the external Cassegrain focus. A 6×6 array of microlenses is located above the science CCD to achieve the necessary photometric precision (see Section 1.5). The filter is a broadband filter with a central wavelength of 525 nm and an FWHM of 300 nm (see Fig.1.3). This custom filter was chosen to gather more photons and thus increase the signal-to-noise (S/N) ratio of the exposures. It does not correspond to any standard filter and therefore it is very difficult to perform a comparison of calibrated intensity.

[2]The system which is responsible for MOST's pointing accuracy is referred to as Attitude Control System (ACS). The ACS originally was designed exclusively to guarantee the necessary pointing accuracy.

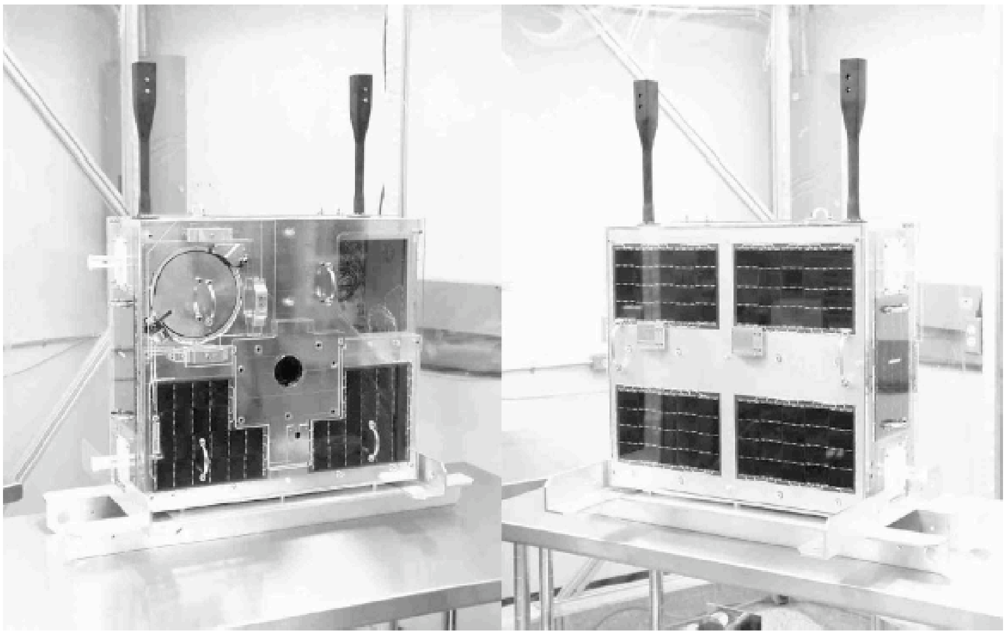

Figure 1.1: Two photographs of the MOST satellite nearing completion at UTIAS. Left panel: Circular aperture for the telescope diagonal (with cover closed), the square opening for the radiant cooling surface, and the area in the center for attachment to the rocket. Right panel: Solar panels covering the opposite side. The two black booms hold the magnetometer sensors sufficiently far from the ferromagnetic Invar of the telescope structure. The satellite is surrounded by a plexiglas box with carrying handles while in the lab (Walker et al. 2008).

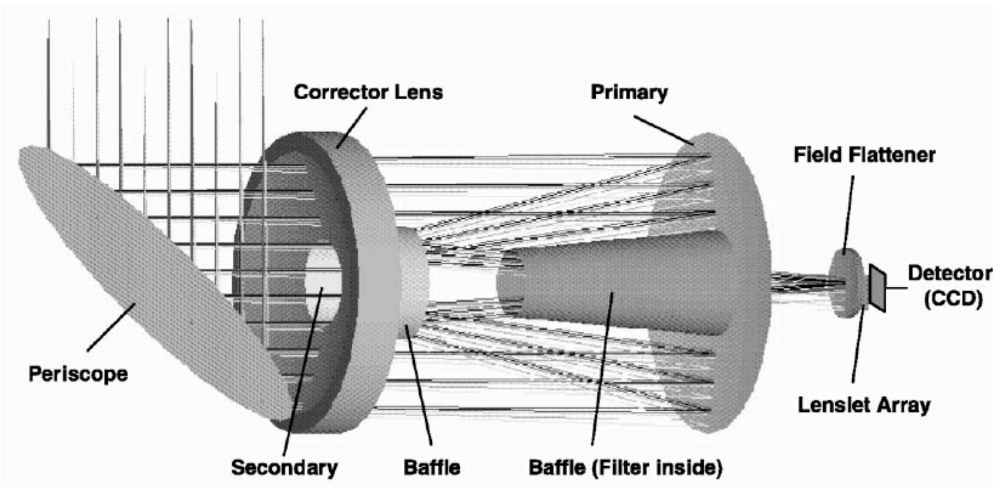

Figure 1.2: Optical layout (Walker et al. 2003).

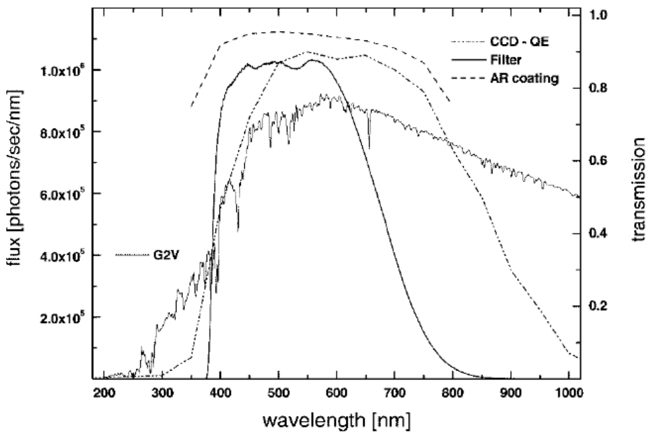

Figure 1.3: Transmission of the MOST filter (solid line) compared to the solar spectrum, the quantum efficiency of the CCD (dashed-dotted line) and the transmission of the coating of the telescope optics (Walker et al. 2008)

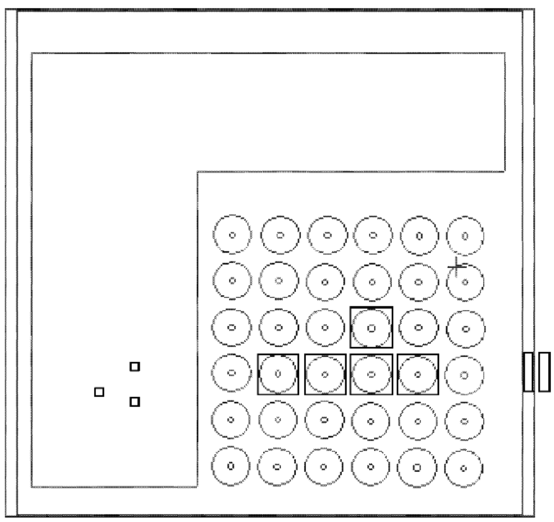

Figure 1.4: The boxes indicate those areas of the science CCD from which data will be captured and sent to ground: two target Fabry images, three "sky" Fabry images, three serendipitous direct images, and two over-scanned regions for bias levels (Walker et al. 2008).

1.5 Detectors and Photometry

MOST uses two 1024×1024 charge coupled devices (CCDs), which rely on the photoelectric effect in semiconductor materials. CCDs convert incoming photons into electrons which are then converted into a digital signal. To reduce the risk in a space mission by redundancy, two frame-transfer CCDs, which allow to start and stop exposures without a mechanical shutter, are used. The main CCD is used for science exposures of the primary program targets, whereas the second has been[3] used by the ACS for guiding and pointing purposes.

1.5.1 The science CCD

A 6×6 microlens Fabry array (Fabry 1927) is positioned above the main CCD. Field stops of 54″ diameter are located to center the incoming light onto one microlens which in turn produces an image (44 pixels diameter) of the entrance pupil on the CCD. This defocused, doughnut-shaped, image is a projection of the primary mirror. The primary advantage of this technology is that the Fabry image remains stable on the CCD even if the ACS would allow a jitter of up to 10 arcseconds. Secondly, pixel-to-pixel variations, which are present on every CCD, can be neglected because the Fabry image is spread over many (≈ 450) pixels. According to Fig.1.6, the Fabry array does not cover the whole area of the science CCD, and the uncovered L-shaped part (12 x 13 mm) of the CCD can be used to obtain direct images of stars. All obtained images are defocused because MOST itself is defocused by +0.15mm. For the purpose of this mission defocused images are favourable because one does not wish to resolve a stellar object but to measure its brightness variations. The targets observed without employing the Fabry lens are called direct imaging targets.

1.5.2 The tracking CCD

The guidance CCD is needed because guide-star information has to be read-out more often and at a much shorter rate than the complete exposure time for a program star to get a high S/N ratio from the science target. Initially no intensity informations of the guide stars could be recorded . This was made possible by some additional software upgrades. For each primary target, photometry of up to about 50 guide stars in the field can be obtained by MOST. Due to the limited downlink capacity, the guide star data are MOSTly processed on board the spacecraft.

A 20×20 pixel raster is placed around each guide star. The background is estimated by averaging the first and last column of the raster. All the signals from pixels in the guide star raster that exceed the background plus a threshold value are summed and comprise one photometric measurement. Integration times range from 0.3 to 3 seconds, but those integrations are stacked onboard in stacks of $10 - 20$ exposures. This results in a typical net sampling rate of 1 to 2 data points per min. Even with such a simple processing scheme, a point-to-point precision of 1 mmag can be achieved for a star of V $\approx$ 7.

1.6 Orbit and satellite communication

In order to select the appropriate orbit for a space mission, there are three arguments to be taken into account:

[3]In early 2006, a strong particle hit knocked out the guidance CCD. Since then, the science CCD is responsible for the satellite tracking

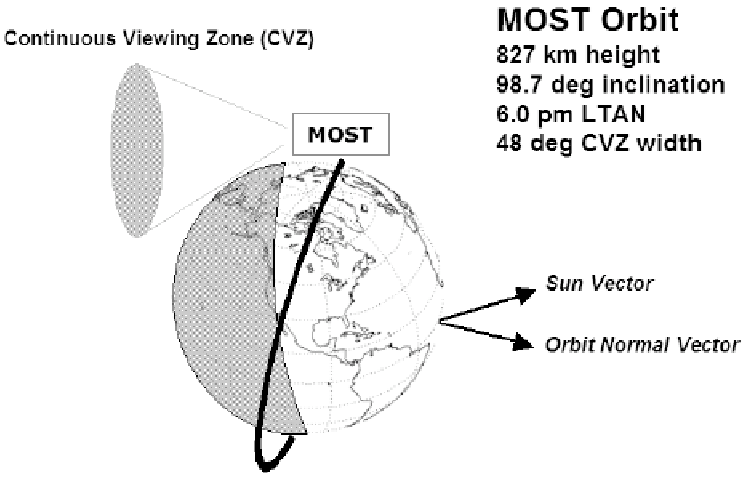

Figure 1.5: MOST's sun-synchronous orbit showing the Continuous Viewing Zone (Walker et al. 2003)

1. the front of the satellite must not be directed towards the Sun,
2. a solar eclipse by the Earth would mean a considerable power loss and result in an inoperable satellite (the higher the orbit, the better),
3. due to the tilt of the Earth's rotation axis with respect to the magnetic axis the inner Van Allen radiation belt reaches its closest approach to the surface at the so-called SAA (South Atlantic Anomaly). This region is a dangerous environment for all satellites and should be avoided if possible (the lower the orbit, the better).

A compromise was chosen and MOST orbits now at an altitude of 820 km in a low-Earth polar orbit with a period of 101.4 minutes. To extend the duty cycle and to achieve an effective and continuous illumination of the solar panels, the inclination of the orbit (98°) was chosen in such a way that the satellite always points to an anti-solar direction without the Earth eclipsing the field. This is achievable if the orbital plane precesses at the sidereal rate and the spacecraft always crosses the terminator (the border between day and night). MOST cannot observe all stars at the same time: the Continuous Viewing Zone (CVZ) is the area where uninterrupted star observations can be achieved. The CVZ is determined by the declination of an object and the sun-sensor zone. The latter describes the angle towards the Sun which must lie within ±30° to keep the satlleite operating. MOST's CVZ ranges from -19° to +36° in which stars can be monitored for up to 60 days without interruption (see Fig.1.5).

MOST transmits the obtained data in two scientific formats, SDS1 and SDS2 (Scientific Data Stream), to Earth. While the SDS1 data stream only contains binned data, the SDS2 data stream includes also pixel intensities and is therefore more voluminous than SDS1. Due to the limited downlink bandwidth only CCD sub-rasters with certain areas are read out and transmitted to Earth. SDS2 contains the Fabry image of interest and its neighboring Fabry images with background information and other areas to determine dark and bias levels (see Fig.1.4). "An essential detail in planning and implementing a satellite mission is the downlink of data back to Earth. For this purpose, MOST uses three different ground stations for communication, one of which is stated

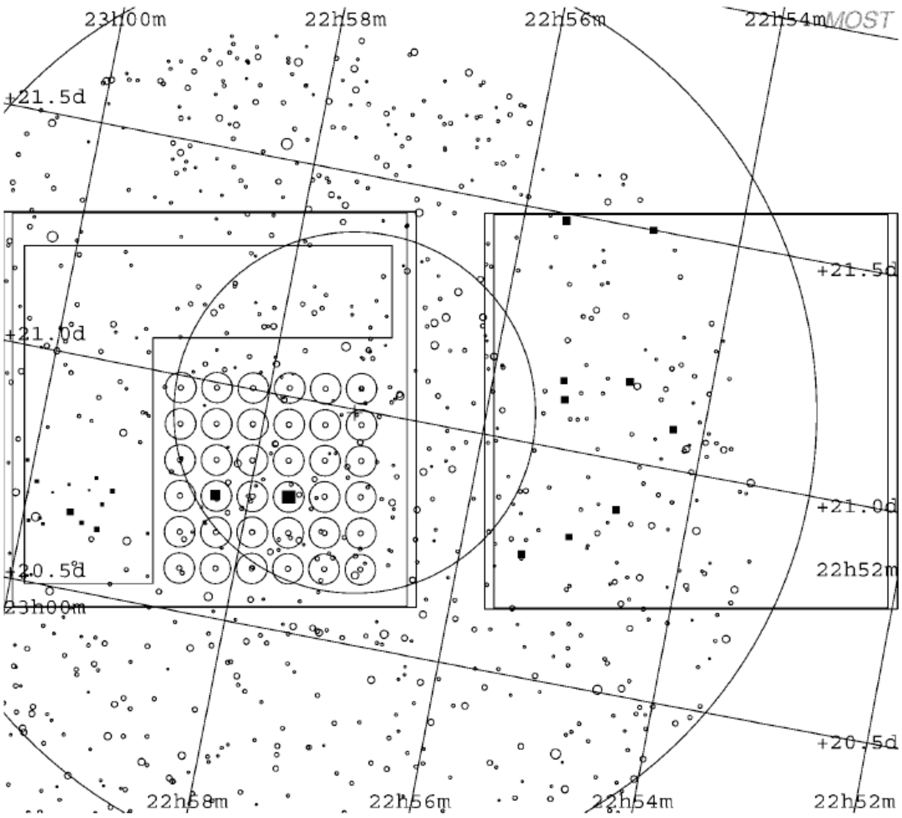

Figure 1.6: Active areas of the guidance and science CCDs are shown superposed on a star field together with outlines of the Fabry lenses and their field stops. The size of a stellar symbol corresponds to its brightness. Filled symbols are stars that will be used for tracking in the guidance field, measured by Fabry photometry in the science field and serendipitously in the open part of the science field. In the example shown here for 51 Peg, a second star actually lands centrally on a neighboring microlens for the appropriate spacecraft orientation (Walker et al. 2003).

at the University of Vienna (the other two being in Toronto and Vancouver, Canada). Considering the size of a full CCD image of 512 kb, one might not expect many problems with downloading the data in times of gigabyte hard drives and megabyte bandwidths. The downlink rate for MOST, however, is only 38 kb/s. Considering that a pass duration over a ground station is normally on the order of 10 minutes and the satellite is expected to collect science exposures at least once per minute, it becomes clear that data processing is a major challenge" (Huber 2008).

Chapter 2

Slowly Pulsating B Stars

2.1 Introduction

This independent class of variable stars was introduced by Waelkens (Waelkens 1991) after a systematic study among B type stars. In 1985 photometric variability in mid-B type stars with a well defined period in the order of a day, variable amplitudes and significant color variations were detected (Waelkens & Rufener 1985). Later it was understood that these stars were the photometric equivalent of 53 Persei stars and that the variations are caused by stellar variations (Waelkens 1987). Although no hints of multiperiodicity were detected, two stars of the observed sample showed a second frequency (Waelkens 1987). It became clear that long data strings were necessary to understand the frequency patterns in these stars.

After seven years of observation the new class of variables was introduced. It would have been appropriate to name these stars as 53 Persei stars, since the line profile variability of 53 Persei was recognized first. Waelkens, however, did not want to name these stars after this prototype star because many of those could be unrelated to the stars he has been observing. Instead he introduced a new class of variables naming them "slowly pulsating B (SPB) stars" (Waelkens 1991).

SPB stars pulsate in high-order, low-degree gravity modes (see Section 2.1.1) with periods of the order of days, showing dense frequency spectra, low amplitudes and multi-periodicity with beat periods of months and even years. SPB stars are hot with effective temperatures between 10000 - 20000 K and masses which range from 3 to 8 solar masses. Their pulsation is probably driven by the κ-mechanism (see Section 2.1.2), i.e. the iron opacity bump. Being trapped deep inside the star, these modes are very promising for asteroseismology (De Cat 2007). Currently, there are at least 50 confirmed SPB stars and 65 candidate SPB stars in our galaxy, 60 in the LMC and 11 in the SMC (Kołaczkowski et al. 2006).

2.1.1 Pressure and gravity modes

There are two ways to excite nonradial oscillations in stars. The first and for this thesis less important one is called pressure- or p-mode (sometimes also called acoustic mode), because the gas pressure is the restoring force. Such modes are present, e.g. in δ Scuti stars and also in our Sun. The p-modes are always found at the high-freqency end of the nonradial oscillation spectrum.

On the other hand there are the gravity- or g-modes, where the buoyancy in the gravitational field is the main restoring force. These modes are present in, e.g., γ Doradus and SPB stars. They are always found at the low-frequency end.

2.1.2 The κ Mechanism

The κ mechanism is believed to be the main driving mechanism for nonlinear pulsations of stars located in the classical instability strip and SPB stars. The opacity κ is the ability for radiation to penetrate through the star. It is is a material function of the form $\kappa = \kappa(\rho, T)$ or $\kappa = \kappa(P, T)$, where ρ is the density, T the temperature and P the pressure in a stellar atmosphere. Since there is no unique approximation for the opacity available that would apply to the whole star, opacity tables for different chemical mixtures are employed (Kippenhahn & Weigert 1990).

The following equations and examples until the end of this subsection are all taken from Hansen et al. (2004), who describe the κ mechanism in a very detailed and understandable way. The κ mechanism can be derived by linearizing the diffusion equation

$$L_r = -\frac{(4\pi^2)^2 ac}{3\kappa} \frac{dT^4}{dM_r} \tag{2.1.1}$$

where L is the luminosity and M the stellar mass.

The relative variation of radiative luminosity is then

$$\frac{\delta L_r}{L_r} = 4\zeta - \frac{\delta\kappa}{\kappa} + 4\frac{\delta T}{T} + \frac{1}{dT/dr} \frac{d}{dr} \left(\frac{\delta T}{T} \right). \tag{2.1.2}$$

Assuming that the variations are adiabatic (which they are in the quasi-adiabatic calculation), neglecting the derivative term and using $\kappa \propto \rho^n T^{-s}$, the linearized mass equation

$$\frac{\delta\rho}{\rho_0} = -3\frac{\delta r}{r_0} - r_0 \frac{\partial(\delta r/r_0)}{\partial r_0} \tag{2.1.3}$$

without the derivative term, and

$$\left(\frac{\delta\rho}{\rho} \right)_{ad} (\Gamma_3 - 1) = \left(\frac{\delta T}{T} \right)_{ad}, \tag{2.1.4}$$

one finds

$$\frac{\delta L_r}{L_r} \approx -\left(\frac{4/3 + n}{\Gamma_3 - 1} \right) \frac{\delta T}{T} + (s+4)\frac{\delta T}{T}. \tag{2.1.5}$$

Equation (2.1.5) is used in the quasi-adiabatic expression

$$\kappa_{qa} = \frac{\int_M (\delta T/T)(\partial \delta L_r/\partial M_r) dM_r}{2\sigma^2 J}, \tag{2.1.6}$$

where J is the oscillatory moment of inertia $J = \int_M \zeta_{ad}^2 r^2 dM_r$.

If κ_{qa} is positive, i.e. the mass gradient of δL_r is positive upon compression, then the star is stable. In a region of the star where ionization is barely active we can set $n = 1$ and $s = 3.5$ (also called Kramers' opacity). If a gas is non-ionized, one can set $\Gamma_3 = 5/3$ which is the common known value for an ideal gas. Using these assumptions one gets $\frac{\delta L_r}{L_r} = 4(\delta T/T)$ and thus gets

$$\frac{\partial \delta L_r}{\partial M_r} \approx 4L_r \frac{\partial(\delta T/T)}{\partial M_r}, \tag{2.1.7}$$

if $\frac{\partial L_r}{\partial M_r} = 0$, which is the case when no energy is generated. The fact that $\frac{\partial(\delta T/T)}{\partial M_r} > 0$ upon adiabatic compression (because variations in density and radius are small near the center and bigger in the outer layers) implies that the mass gradient of δL_r must also be positive and therefore κ_{qa} is positive. In physical terms, this means that if a mass shell is compressed, more radiative power comes out of it than is entering it. The star is stable.

However, in an active ionization layer (e.g. second helium ionization zone), where κ decreases slowlier ($s \ll 3.5$) or actually increases with temperature and $\Gamma_3 < 5/3$ due to the fact that the gas is ionized, the situation looks different. It can happen that the mass gradient of δL_r is negative when δT is positive. In contrast to what happens in the case above, a mass shell gains heat when it is being compressed. The increase in opacity inhibits the normal radiative flow and therefore the mass element heats up. This effect can be compared with a thermodynamic heat engine, where energy is taken from the system during the hot phase and again released in the cold phase, therefore driving occurs. The star is unstable (Aerts 2004).

This somewhat illogical condition, that the κ mechanism requires an increase in opacity while the temperature increases, is only fulfilled in regions of the star where hydrogen and helium are ionized. The boundaries of the classical instability strip in the Hertzsprung-Russel diagram (HRD) where all stars are expected to show pulsation are set by the occurrence of these ionization regions in the appropriate layers.

2.2 Frequencies

De Cat (2007) shows the frequency distribution of confirmed and candidate SPB stars in Fig.2.3. As he points out, most of the observed frequencies lie below 1.5 d^{-1}, which is consistent with the frequency range of the predicted unstable SPB modes (Dziembowski et al. 1993). For the confirmed SPB stars, the frequency distribution peaks at 0.65 d^{-1}, whereas for the candidates it peaks around 1.10 d^{-1}. De Cat (2007) assumes that some 20% of the candidate SPB stars could be misclassified because the SPB like frequency could be due to rotational modulation or binarity, which is why one needs high resolution spectra to solve this problem.

2.3 Amplitudes

De Cat (2007) is aware that it does not make much sense to compare the amplitude distributions in the panels in Fig. 2.4 because they base on observations in different filters. He states, however, that the amplitudes have a pronounced maximum at a few hundredths of a magnitude. The most obvious fact in this figure is the difference in ground-based (top left, top right, bottom right panels) and space-based observations (MOST observations in the bottom left panel): he points out that no amplitudes below $\sim$ 1 mmag can be observed from Earth due to the technical limitations. This shows the importance of MOST and space missions in general which can help us to understand stellar variability in full detail (De Cat 2007).

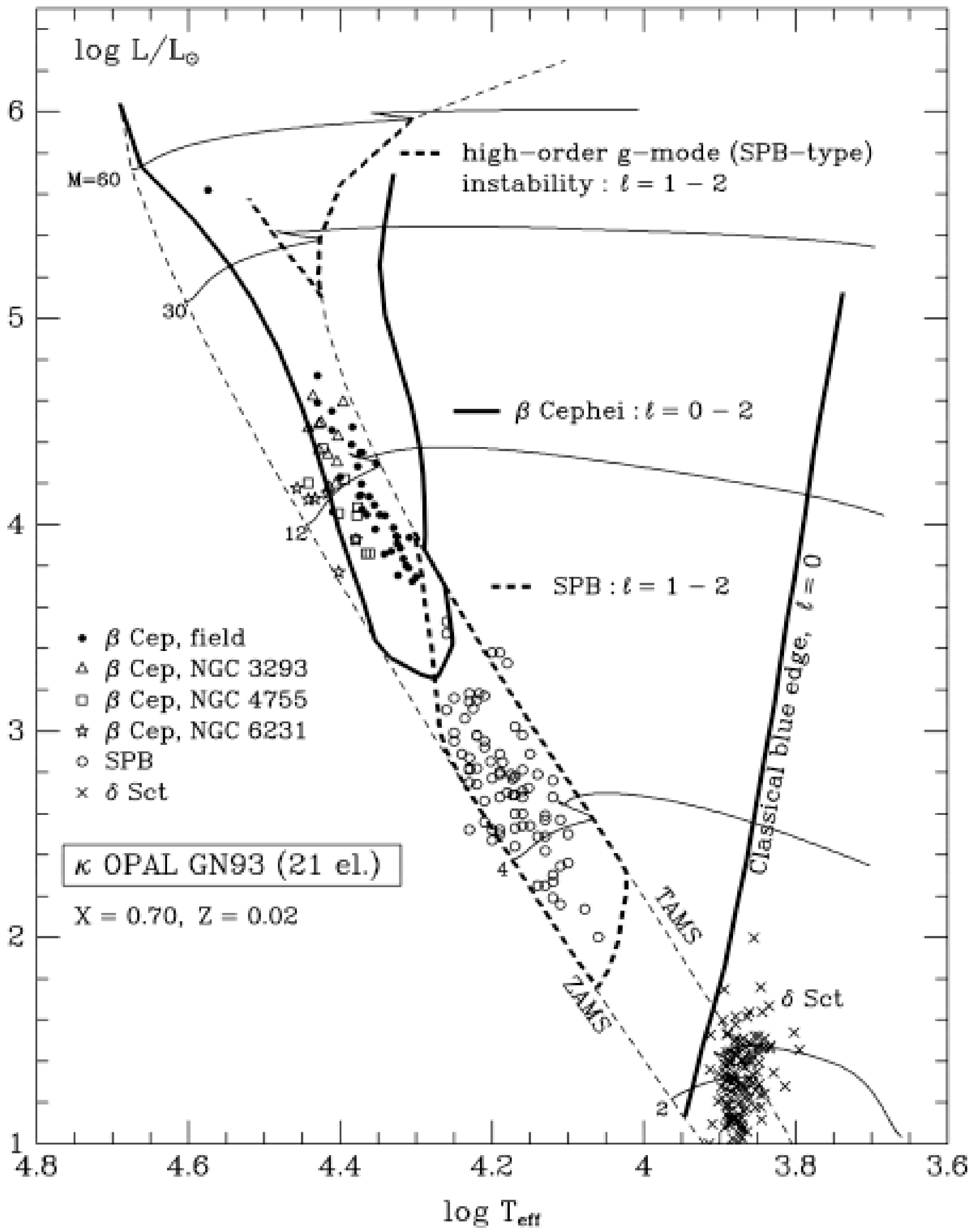

Figure 2.1: HR diagram of the upper main sequence. Five evolutionary tracks and the blue edge of the classical instability strip are shown (Pamyatnykh 1999).

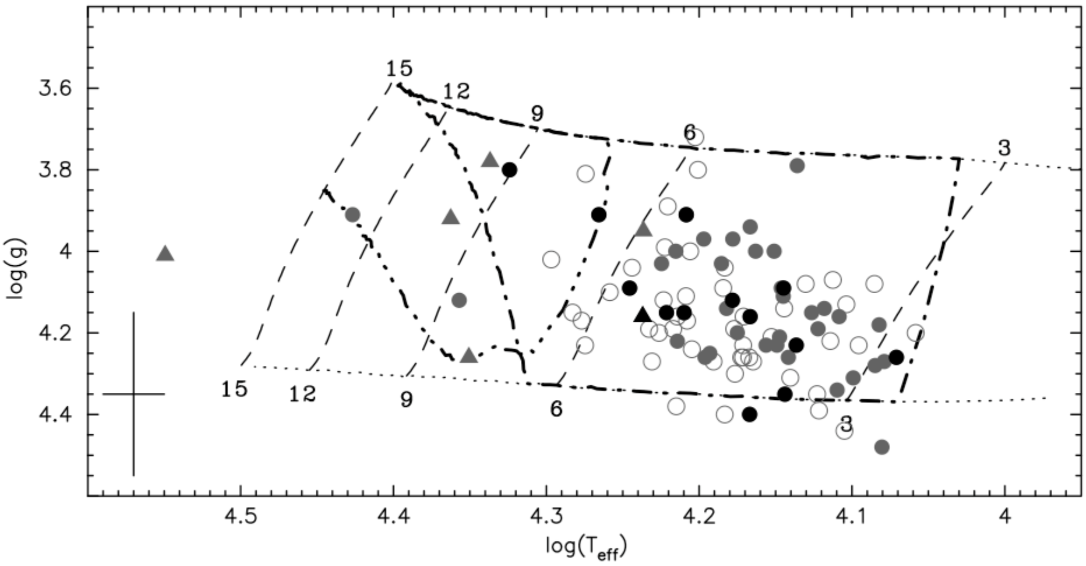

Figure 2.2: Positions of the candidate (open symbols) and confirmed (full symbols) SPB stars in the (log($T_{\rm eff}$), log g)-diagram for which Geneva photometry is available. Hybrid β Cep/SPB stars are indicated by triangles. The lower and dotted lines indicate the ZAMS and TAMS respectively. Evolutionary tracks for stars with M=15, 12, 9, 6, 3 solar masses are shown as dashed lines. The theoritcal β Cep instability strip is shown as a dashed-dotted-dotted-dotted line, the SPB instability strip as dash-dotted line. The error bar is given in the lower left corner. (De Cat et al. 2007)

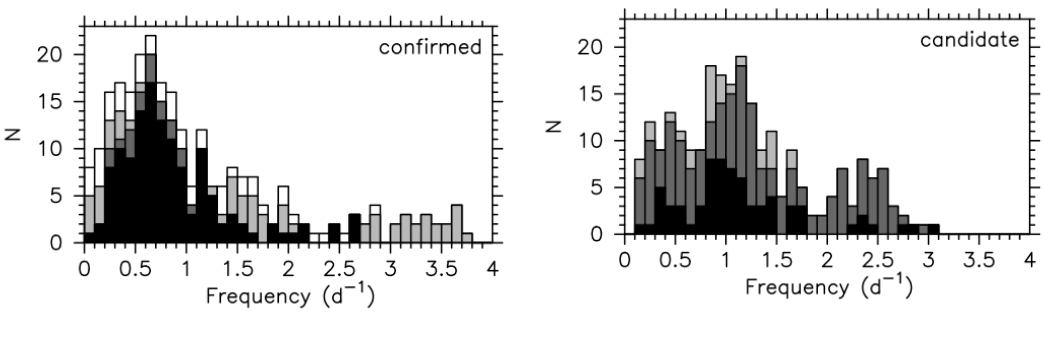

Figure 2.3: Left: Frequency distribution of the confirmed SPB stars based on ground-based observations of confirmed members (black) and on the MOST observations of HD 163830 (dark gray), HD163868 (light gray), and HD 163899 (white). Right: Frequency distribution of galactic (black) and extragalactic (LMC: dark gray and SMC: light gray) candidate members. (This figure was kindly provided by De Cat (2007)

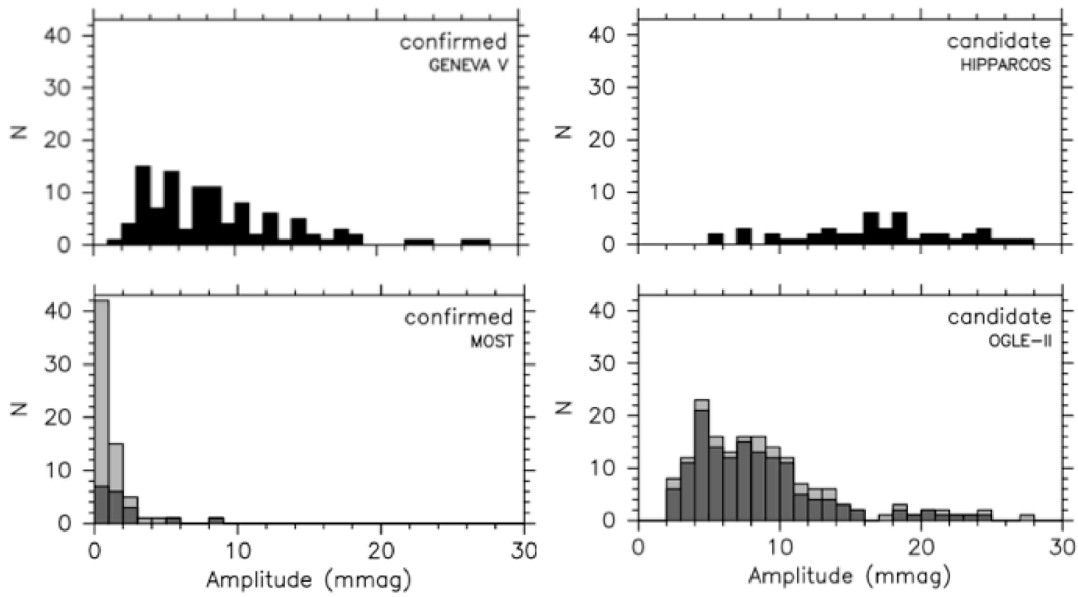

Figure 2.4: Amplitude distribution in photometry. Left: Geneva V photometry of confirmed members (top) and on the MOST observations of HD 163830 (bottom, dark gray) and HD 163899 (bottom, light gray). Right: based on the Hipparcos H_p observtions of candidate glactic members (top) and the OGLE-II observations of candidate members in the LMC (bottom, dark gray) and the SMC (bottom, light gray). (Figure provided by (De Cat 2007))

2.4 Chemical composition

Niemczura (2003) observed 34 reference and 20 SPB stars and determined their metallicity based on low-resolution IUE spectra. The average metallicity of $Z \approx 0.013$ was nearly the same in the pulsating and non-pulsating stars. With this quite low metallicity some low frequency modes could be explained (De Cat 2007).

A still ongoing study tries to determine NLTE abundances of the majority of all confirmed slowly pulsating B stars. First preliminary results of the SPB star HD 85953 show that the chemical abundances are indistinguishable from OB stars in the solar neighborhood whereas HD 3360 shows boron depletion and a clear nitrogen excess which is also common in β Cep stars (Briquet & Morel 2007).

2.5 Rotation

In Fig.2.5 De Cat (2007) presents the distribution of the projected rotational velocity ($v \sin i$) for confirmed and candidate SPB stars. He emphasizes that SPB pulsations are not restricted to slow rotators. However, one has to expect significant frequency shifts for non-zonal modes ($m \neq 0$, see Section 3.1) in rapid rotators, which has to be considered in asteroseismic modeling of these stars. It is likely that the amplitudes depend on rotation, as one notices that the amplitudes of confirmed SPB stars decrease for higher $v \sin i$ values. De Cat considers this interpretation as a possible sample-size effect because the slow rotators were chosen first for follow-up spectroscopic

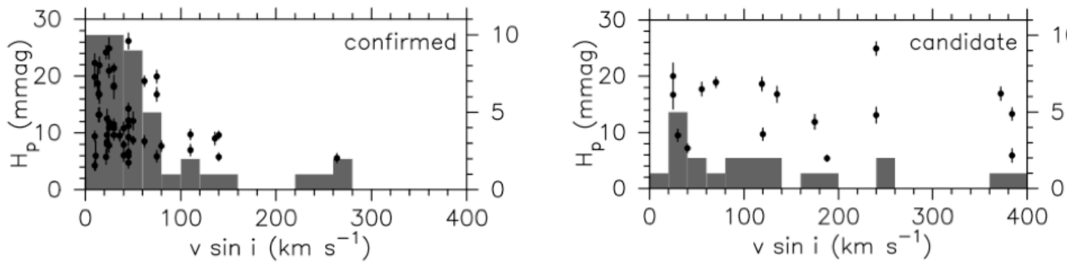

Figure 2.5: Distribution of the projected rotational velocity ($v \sin i$) for the confirmed (left) and candidate (right) SPB stars. The dots with error bars denote the amplitudes of the observed frequencies in the Hipparcos H_p filter. (This text and figure was kindly provided by (De Cat 2007))

studies. The right panel of Fig.2.5 indicates that SPB stars with high photometric amplitudes exist, and only additional observations can confirm or reject them as pulsating stars.

2.6 Magnetic fields

HD 3360, a SPB star with a rotation period $P_\Omega = 5.37\,\mathrm{d}$ and a pulsation frequency of $0.64\,\mathrm{d}^{-1}$, has a polar magnetic field of $B_{pol} = 335^{120}_{-65}\ G$ whose longitudinal component varies sinusoidally with P_Ω (Neiner et al. 2003). Assuming a simple dipolar configuration this magnetic value corresponds to a polar field of 110 kG in the surroundings of the convective core, which in turn can cause a frequency splitting of 1% for a g^1_{20}-mode (Hasan et al. 2005). More longitudinal magnetic fields of a few hundred Gauss were detected in another 13 SPB stars (Hubrig et al. 2006). These low magnetic fields can explain the very close frequency multiplets observed in some SPB stars.

Chapter 3

Stellar modelling

Thanks to the pulsational stability analysis performed by Hideyuki Saio more significant insights of the observed stars can be found, i.e. if a mode is excited or damped. Saio's code is based on the method of Lee & Baraffe (1995) who include the Coriolis force, i.e. the first order effect of rotation, and, more importantly, the centrifugal force, i.e. the second order effects of rotation. The equation of hydrostatic equilibrium becomes:

$$\frac{dP}{dr} = -g\rho + \frac{2}{3} r\Omega^2, \tag{3.0.1}$$

where P is the pressure, r the distance from the center, g the local gravitational acceleration, ρ the density and Ω the angular frequency of rotation which is assumed to be constant throughout the interior and the life of the star.

3.1 Radial and non-radial oscillations

The radial oscillations is the simplest form of a stellar oscillation. Such an oscillation preserves spherical symmetry, i.e. the star expands and contracts radially. The smallest frequency in a radial oscillation is the fundamental frequency. One can deduce the mean density of a radial oscillator, e.g. Red Giant, RR Lyrae star by using

$$P \propto \frac{1}{\sqrt{\bar{\rho}}}, \tag{3.1.1}$$

where P is the period of the fundamental mode and $\bar{\rho}$ the mean density of the star. Radial oscillations are usually denoted with a n, the number of nodes between the center and surface of the star.

Non-radial oscillations involve both radial and horizontal motions in stars. One can expand the angular dependence of an amplitude of a pulsation frequency in spherical harmonics $Y_l^m(\theta, \phi)$, where m and l describe the dependence of the mode on θ and ϕ.

$$Y_l^m(\theta, \phi) := \sqrt{\frac{2l+1}{4\pi} \frac{(l-m)!}{(l+m)!}} P_m^l(\cos\theta) \exp(im\phi), \tag{3.1.2}$$

where

$$P_l^m(x) := \frac{(-1)^m}{2^l l!}(1-x^2)^{m/2}\frac{d^{l+m}}{dx^{l+m}}(x^2-1)^l, \tag{3.1.3}$$

is the associated Legendre function (Aerts 2004).

However, only for a non-rotating, spherical star, the spheroidal motion is proportional to a single Y_l^m. Every star rotates and therefore one has to implement toroidal motion as well. Unluckily one cannot express both, the spheroidal and toroidal motion, with one Y_l^m alone. The solution to this problem lies in the expansion of an even mode using Y_l^m with $l = |m| + 2j - 2$ for the spheroidal and $l = |m| + 2j - 1$ for the toroidal motion($j = 1, 2, ...$). Odd modes, on the other hand, can be expanded with $l = |m| + 2j - 1$ for the spheroidal and $l = |m| + 2j - 2$ for the toroidal motion (Saio et al. 2007). For the special case that $l = 0$ the mode is simply a radial oscillation, thus being a special case of the non-radial oscillation.

m-modes are nodal lines which are crossing the rotation axis of the star. In this thesis it is assumed that positive m-values are modes that move in the opposite direction of rotation and are thus retrograde modes. Negative m-modes are therefore moving in the direction of rotation and are called prograde modes.

If the spherical harmonic order m is equal to zero, the spherical harmonic function $Y_l^m(\theta, \phi)$ does not depend on longitude, i.e. that there are no nodes crossing the rotation axis (see Fig.3.1). In this case the modes are called 'zonal' modes. On the other hand, if $l = |m|$, the modes are called 'sectoral', i.e. there are only nodes which are crossing the rotation axis. In any case $l \geq |m|$ (Aerts 2004).

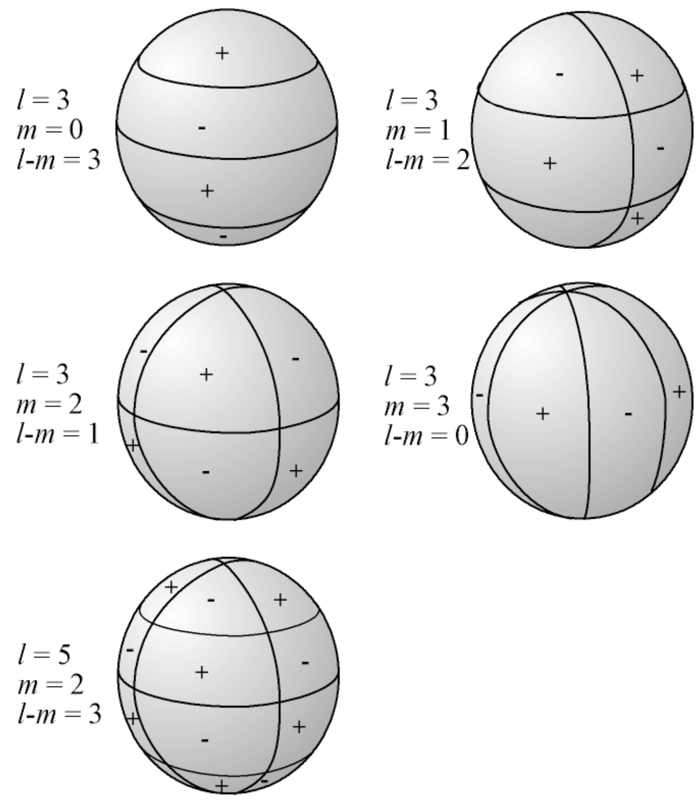

Figure 3.1: Representation of the spherical harmonic function Y_l^m. The positive sign indicates the expansion, the negative sign the contraction of the star.

Chapter 4

Frequency Analysis

In the following sections I will try to give an overview of the software and tools used for the frequency determination of the observed guide stars. This will mainly be based upon the master thesis by Daniel Huber (2007), University of Vienna, who gave an excellent summary of available techniques and strategies. For a low-amplitude signal from a star it is very difficult, if not impossible, to determine the frequencies from the light curve with the naked eye. Stellar, i.e. intrinsic, oscillation is usually not the only signal contained in a light curve. There is always instrumental noise present in Most data, causing an increased scatter of datapoints and even pulsation in more than one frequency is thinkable. This makes it impossible to distinguish intrinsic frequency components from the combined beating effects seen in the data without specific tools.

4.1 Fourier analysis and Discrete Fourier Transform (DFT)

A popular technique is Fourier analysis, i.e. the representation of a given light curve or any other function as an infinite number of sines and cosines at different periods and amplitudes. A modification of Fourier analysis, the Discrete Fourier Transform (DFT) (Deeming 1975), considers the spectrum as a continuous function of frequency. Peak-finding in such a DFT amplitude spectrum allows to determine, or at least estimate, the eigenfrequencies of the star or of the examined source.

In principle, the DFT should attain a local maximum at some frequency if the data contain a corresponding coherent signal. If there is more than just one signal present, one expects the DFT to attain local maxima at each frequency with the highest amplitude at the frequency with the highest peak.

4.2 Noise

In the context of DFT and Fourier analysis, one should never forget to mention noise. Regardless of the quality of the measurements and the instruments used for the observation, both photon noise and measurement errors are always present.

Photometric measurements, such as those used in this thesis, are limited to photon statistics according to a Poisson distribution. This means that the noise simply is the square root of the number of detected photons. The more photons, the better the measurement and the higher the signal-to-noise ratio. Although the noise decreases, it never disappears. The DFT treats intrinsic signal, sky background and instrumental effects, as signal. Therefore one will always find noise in the Fourier spectrum. However, noise is not a negative aspect at all. Rather, the signal-to-noise ratio, is a very important feature of Fourier analysis, because it allows to determine the reliability of the results.

4.3 DFT-based methods

The DFT is surely the simplest of all available algorithms. It interprets the Fourier integral as a finite sum over data points. The main advantage of this method is that it is able to calculate the Fourier transform of non-equidistantly spaced data points. Because of this, more sophisticated methods and algorithms, e.g. the Lomb-Scargle periodogram (Scargle 1982), are based on the DFT. The major drawback of the DFT is the computation time, which increases proportionally to the square of the number of data points. The first who found a way around this problem was Gauss, and later Danielson and Lanczos (1940s) discovered a way such that the computation time increases only with $N \log_2 N$, with N being the number of data points. This method is known as the Fast Fourier Transform (FFT) (Brault & White 1971). However, the condition to use this algorithm, is equidistant data sampling. In astronomy, especially in photometry, equidistant data sampling is simply not achievable in most cases. Theoretically one could re-grid the data, which in turn would introduce additional errors. For that reason the FFT is not an option for astronomical time series analysis.

4.4 SigSpec

The SIGnificance SPECtrum was mainly used for the data analysis in this master thesis, and I shortly want to outline the basic properties and the advantages of this method. SigSpec is a frequency analysis tool based on the Fourier analysis technique, developed by Reegen (2007).

As pointed out earlier in this chapter, a recorded signal is a superposition of an intrinsic stellar signal and multiple other effects, as for example instrumental periodicities caused by e.g. thermal effects. It is crucially important to know or at least estimate if a peak is generated by noise or by intrinsic stellar signal because this choice influences the prewhitening sequence, meaning the subtraction of a signal component from the light curve and doing another Fourier analysis of the residuals. A poor choise can influence the whole result and thus make it wrong and unusable. On top of that, even Gaussian noise can cause amplitude peaks in the DFT spectrum (Scargle 1982). The amplitude of such a noise-generated peak is arbitrary and in the worst case it can be as high as, or even higher than the stellar amplitude. The probability that the highest peak in the spectrum is caused by white noise is higher for low-amplitude peaks. This probability is called the False-Alarm Probability Φ_{FA} and relies on the Probability Density Function (PDF) which is a tool to calculate the probability of a random variable between to real numbers, i.e. $P[a < x < b] = \int_a^b f(x)dx$.

The PDF of a time series $x_k = x(t_k)$ representing Gaussian noise is then

$$\phi(x_k) = \frac{1}{\sqrt{2\pi\langle x^2\rangle}} e^{-\frac{x_k^2}{2\langle x^2\rangle}} \tag{4.4.1}$$

with $\langle x^2\rangle$ being the population variance.

According to Reegen (2007) the PDF of the time domain can be transformed into the PDF of the frequency domain, which results in

$$\phi(A' \,|\omega, \Theta) = \frac{A}{2\pi\sqrt{\langle\alpha^2\rangle\langle\beta^2\rangle}} e^{-\frac{A^2}{8}\left[\frac{\cos^2(\Theta-\Theta_0)}{\langle\alpha^2\rangle} + \frac{\sin^2(\Theta-\Theta_0)}{\langle\beta^2\rangle}\right]} \tag{4.4.2}$$

where (A, Θ) are the polar coordinates, $\alpha = \frac{A}{2}\cos(\Theta - \Theta_0)$ and $\beta = \frac{A}{2}\sin(\Theta - \Theta_0)$.

Now one can calculate the False Alarm probability Φ_{FA} by integrating (4.4.2) as follows

$$\Phi(A \,|\omega, \Theta) = \int_0^A dA' \, \phi(A' \,|\omega, \Theta) \tag{4.4.3}$$

Reegen introduces the so-called spectral significance which is given by

$$sig(A \,|\omega, \Theta) := -\log \phi_{FA}(A, \Theta). \tag{4.4.4}$$

A spectral significance of e.g. 5 means that the probability of an observed peak to originate from noise is 1:100000.

Classical signal-to-noise estimates are an approximation to the spectral significance according to

$$sig(A) \approx \frac{\pi \log e}{4} (S/N)^2 \tag{4.4.5}$$

A signal-to-noise ratio of 4, as suggested by Breger et al. (1993) roughly corresponds to a spectral significance of

$$sig(S/N = 4) \approx 4\pi \log e \approx 5.46 \tag{4.4.6}$$

SigSpec exceeds the capabilities of Discrete Fourier Transform (DFT), Phase Dispersion Minimization (Lafler & Kinman 1965) and other mechanisms in various respects:

> "SigSpec does not compare one peak amplitude to another. Thus it avoids implications to the statistical independence of peaks in the amplitude spectrum at a single prewhitening stage and the ambiguity in defining a Nyquist Frequency [...]"
>
> "SigSpec is based on an analytically straight determination of the amplitude Probability Density Function. Provided the noise is white [...], SigSpec returns exact results instead of signal-to-noise estimates.[...]"
>
> "SigSpec is the first technique in astronomical time series analysis to use both frequency and phase angle in the computation of the False-Alarm Probability [...]. The statistics employed by SigSpec takes into account all available information provided by the Discrete Fourier Transform."
>
> "[...] For strong signal components, the peak frequencies returned by SigSpec are considerably more accurate than the solutions of all compared methods. For weak signal components, SigSpec still provides a slightly higher accuracy. [...]"
>
> "Signal-to-noise ratio- based period detection is a matter of experience and - to some - extent -personal taste. SigSpec provides a solution that is completely free of subjective influence. Interpretation is no longer part of the analysis, and the results remain exactly the same, if two different persons apply the calculation to the same data." (Reegen 2007)

4.5 Frequency resolution

In order to estimate the error of a frequency, one can use the Rayleigh frequency resolution

$$\sigma_{Rayleigh} = \frac{1}{T}, \tag{4.5.1}$$

where T is the total time length of the observation run. Although useful, this approach usually overestimates the true frequency uncertainty. For an adequate error estimate in frequency the following method, described by Kallinger et al. (2008), was used in this thesis

$$\sigma_{Kallinger} = \frac{1}{T \cdot \sqrt{sig}}, \tag{4.5.2}$$

where sig is the "spectral significance" obtained with SIGSPEC (see Section 4.4).

4.5.1 CINDERELLA

CINDERELLA, an acronym for "Comparison of INDEpendent RELative Least-square Amplitudes", is an addtional software package to SIGSPEC. It was developed by Reegen et al. (2008).

SIGSPEC refers to uncorrelated, i.e. white, noise. CINDERELLA, on the other hand, compares individual amplitudes and phases in the DFT of a target and one ore more comparison datasets, which can be either stars or sky background (or both) to determine if one ore more peaks are related to any physical process other than stellar signal. In other words, it checks if periodicities that are found in the target data are unique to the target star. Evidently, the observing conditions should be the same or at least similar for all the data sets and the comparison star(s) should show different pulsational behaviour, i.e. the frequencies should be different.

Due to the fact that the data sets do not have the same mean intensity one can not compare these sets directly. CINDERELLA takes this effect into account and recalculates the "amplitude in a target star corresponding to artificial intensity variations of amplitude[s] [...] in a comparison star" (Reegen et al. 2008).

CINDERELLA returns a value, called the conditional spectral significance, which describes the probability that a peak in the target data set is not deterministically related to a peak in a comparison data set. CINDERELLA is, in other words, the replacement of an instinctual evaluation of differential photometry by a more or less experienced observer, with a statistically accurate procedure based on pure mathematics.

Chapter 5

MOST SPB candidates

Among the guide stars observed by MOST, 27 possible SPB stars were identified and are divided into categories A (table 5.1), B (table 6.1) and C (table 6.2). They show significant variability in their light curves and amplitude spectra. In addition, these stars are classified as B stars in the SIMBAD astronomical database. For this master thesis however, only the six stars listed in table 5.1 were analyzed intensively because either Strømgren and/or Geneva multicolor photometry is available (see Fig.5). Category-B stars show multiple periods of the order of a day in their light curves. Unfortunately, no additional measurements exist for these stars and one has to rely solely on the spectral type accesible on SIMBAD. Since the author thinks that SIMBAD is rather unreliable, it is, at this point, not clear if they are SPB stars at all. They could also be γ Doradus stars which show the same behaviour in the light curve but differ significantly in effective temperature. Nevertheless, the light curves, amplitude spectra and the significant frequencies are shown. Additionally to these stars, there are other stars which were observed by MOST also categorized as B stars in SIMBAD. These in turn do not show such obvious signs of multiperiodicity in their light curves, due to e.g. massive data gaps, intensity steps, etc. The significant frequencies of category-C stars were used for statistic purposes explained in more detail at the end of the next chapter.

All stars are relatively faint with magnitudes ranging from as bright as $7^{\mathrm{m}}.64$ for HD 32884 and as faint as $10^{\mathrm{m}}.9$ magnitude for GSC 00154-00785. The spectral types range from very early (B0pe) to very evolved (A0) B type stars which is advantageous if one wants to investigate changing patterns in e.g. the Fourier spectra over the whole temperature range of B stars.

GSC identifier	other ID	spectral type	mag	RA [°]	DEC [°]
GSC 00154-02436	HD 259481	B8	9.27	6 33 43.26	4 55 54.5
GSC 00154-00785	n.a.	B9V	10.9	6 33 35.7	5 16 41
GSC 00750-01778	HD 261810	B1/B8V-B5V	9.15	6 40 43.22	9 46 01.71
GSC 00750-01876	HD 261878	A0-B5V	9.2	6 40 51.55	9 51 49.39
GSC 00750-01119	HD 47469	B5V-B3V	7.8	6 39 11.17	9 38 45.47
GSC 09007-02387	HD 127696	B7III/IV	9.13	14 35 8.23	-61 01 28.27
GSC 00154-01871	n.a.	B5V	11.26	6 33 43.26	4 55 54.5

Table 5.1: Category A: guide stars with known or deduced effective temperature and surface gravity either from Strømgren or Geneva multicolor photometry.

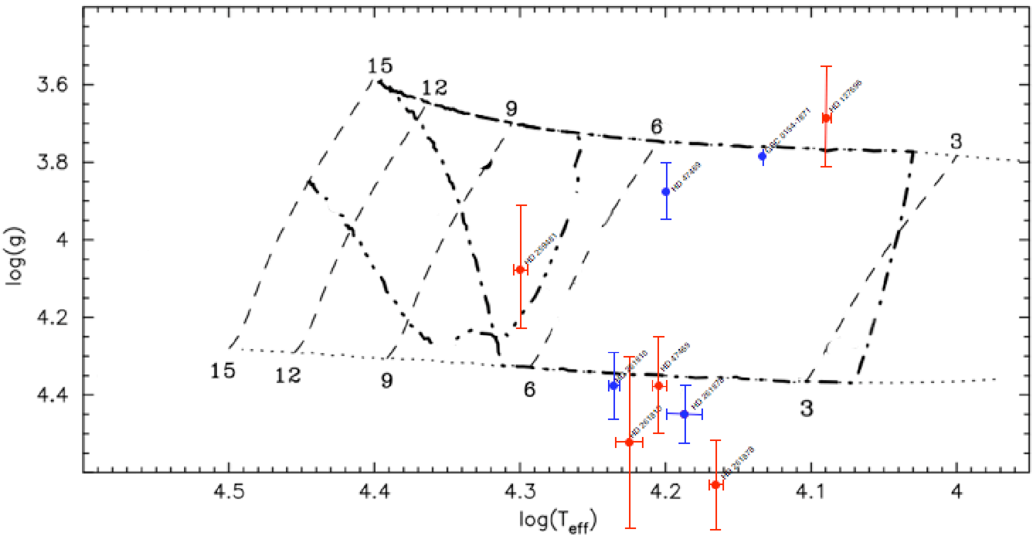

Figure 5.1: Shown in this viewgraph are the positions of the candidate SPB stars in the ($\log(T_{\rm eff})$, $\log g$)-diagram for which Geneva (red) and Strømgren photometry (blue) is available (also listed in table 5.1. The lower and dotted lines indicate the ZAMS and TAMS, respectively. Evolutionary tracks for stars with M=15, 12, 9, 6, 3 solar masses are shown as dashed lines. The theoritcal β-Cep instability strip is shown as dash-dot-dot-dotted line, the SPB instability strip as dash-dotted line (provided by De Cat et al. 2007).

5.1 GSC 00154-02436

GSC 00154-02436 (HD 259481), the 27th guide star in the NGC 2244 run, is identified to star nr. 353[1] in the young open cluster NGC 2244 with a probability of 35% (Kharchenko et al. 2005). The star has a visual magnitude of $9^{m}.27$ (Turner 1976) and is classified as a B star in the SIMBAD astronomical database, and more accurately as a B2Ve star in the "Catalog of Hα emission stars in the northern Milky Way" (Kohoutek & Wehmeyer 1999). This should indicate a SPBe star.

HD 259481 was monitored for approximately 22 days by the MOST satellite in late December 2007 and MOST of January 2008. See Fig.5.2 for the light curves of HD 259481 and the two comparison stars.

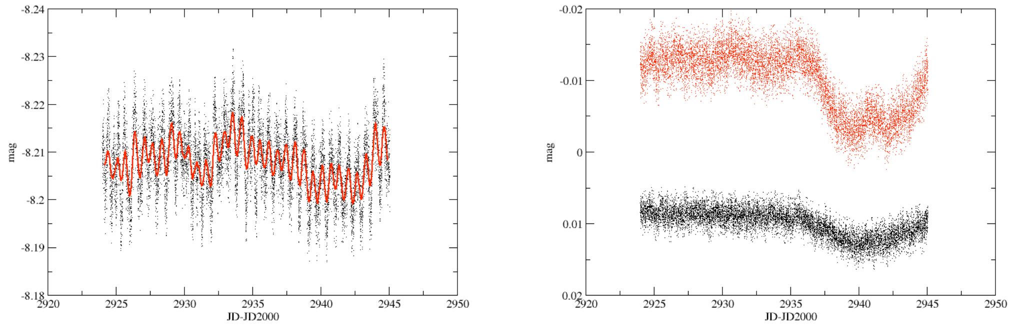

Figure 5.2: Left: Light curve of HD 259481 monitored over 21 days by MOST. In red color a moving average is shown. Right: Light curves of GSC 00154-01521(HD 46202, black) and in GSC 00154-02077 (HD 259480, red). The magnitudes are normalized and set off by +0.01 mag and −0.01 mag, respectively for better visibility. Notice the drop in magnitude in the middle of the observation run.

For this star both *UBV* (Turner 1976) and Geneva photometry (Burki et al. 1999) are available. Since no dereddened *UBV* values are obtainable, the six values of Geneva photometry, *U*: 0.803, *V*: 0.69, *B1*: 0.882, *B2*: 1.51, *V1*: 1.404, *G*: 1.804, together with the Fortran 77 code "calib.f", based on Kurucz models and written by Kunzli et al. (1997), were used to determine the ective temperature $T_{\rm eff}$ and the surface gravity $\log g$. This calibration method yields $T_{\rm eff} = 19956 \pm 217\,{\rm K}$ and $\log g = 4.07 \pm 0.16$. As one can see in Fig.5, the star lies perfectly in the instability range of SPB stars. These findings are not in perfect agreement with the values from Huang & Gies (2006), who find $T_{\rm eff} = 20626 \pm 310\,{\rm K}$ and $\log g = 3.850 \pm 0.038$. The temperature is off by 300° K, which is negligible for hot stars. However, the surface gravity on the other hand is lower by $\sim 0.2\,{\rm dex}$. As we shall see later, these latter values are in perfect agreement to the model fit calculated employing the frequencies obtained from the MOST photometry. Maybe Geneva photometry is not suitable for emission line stars.

5.1.1 Comparison stars

For this star HD 259480 and HD 46202 were used as comparison stars:

HD 259480 is classified as a B8 star in the SIMBAD astronomical data base (α: $6^h\,32^m\,58.6^s$ and δ: $5°\,2'\,1''$) and is, with a probability of 97%, a member of the open cluster NGC 2244 (identified to star nr. 348) (Marschall et al. 1982).

[1] The adopted enumeration for this cluster according to Ogura & Ishida (1981)

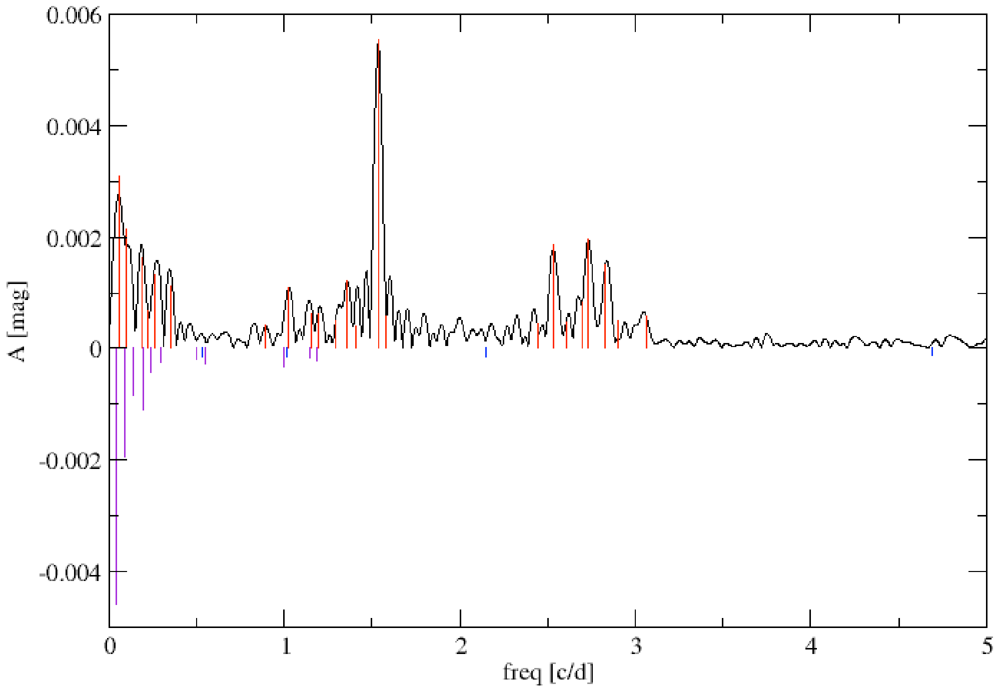

Figure 5.3: Region of interest of the amplitude spectrum of HD 259481 (black) with the identified frequencies (red) and identified frequencies of the two comparison stars HD 259480 and HD 46202 (violet and blue, respectively). For better visibility, the inverted amplitude axis is used to display the comparison star amplitudes.

HD 46202 is classified as an O9V star in the SIMBAD astronomical data base (α: $6^h\,32^m\,10.4^s$ and δ: $4^\circ\,57'\,59.8''$) and is identified to nr. 180 in the open cluster NGC 2244, with a probability of 93% (Marschall et al. 1982). The light curve for both stars is given in Fig. 5.2. As one can see, there is a relatively steep drop in magnitude shortly after the middle of the observation run in both light curves. This is probably caused by either an instrumental effect (temperature variations) or the Moon.

One can see this drop in magnitude also in the target light curve and thus it is highly likely that it is not an intrinsic stellar signal. It is obvious from the light curve that this frequency corresponds to one cycle in 25 days, i.e. we expect to see a frequency in the amplitude spectrum of both the target star and the comparison stars close to 0.04 c/d (which is, by pure coincidence, exactly the Rayleigh resolution of the amplitude spectrum $R = 1/T$ (where T denotes the length of the data set). Because of the arguments mentioned in this paragraph, CINDERELLA should identify and flag this frequency and eventual harmonics.

The amplitude spectrum (Fig.5.3) shows the frequencies and corresponding amplitudes as given in in Table 5.2. Already for the naked eye it is visible that almost all the frequencies below $0.2\,\mathrm{d}^{-1}$ are present both in the amplitude spectrum of the target star and the two comparison stars. As the amplitudes of the comparison stars show a similar value to those in the HD 259481 spectrum, one must assume that these are due to the instrumental effect mentioned above and can thus not be used for modeling the star.

Interestingly enough, CINDERELLA, does not flag these frequencies at all. One can explain this by the fact that significance of the peaks in the target star is so high that CINDERELLA considers these peaks to be intrinsic. However, CINDERELLA indicates the frequencies 1.01 c/d, 17.19 c/d, 12.19 c/d, 1.19 c/d to be present in one comparison data set and the frequency 16.18 c/d to be present in both of the compared data sets.

The frequencies 12.19, 16.18 and 17.19 c/d are related to MOST's orbit period, which is 101.4 minutes (see chapter 1) or, 14.19 c/d. Such peaks, regularly spaced by multiples of 1 c/d around the orbit frequency, are a known problem of the MOST satellite. The peaks around 1 c/d are due to the daily changes of the terrestrial albedo $a(\lambda, \beta)$. Also weather variations, e.g. cloud formations over the Earth which are reflecting more or less stray light onto the detector and thus modulating the light curve, are responsible for this peak in the amplitude spectrum.

The frequencies 0.057 c/d and 0.103 c/d correspond to a period of 17 d and 9.7 d, respectively, which is (half) the length of the data set. In principle, these two frequencies could be intrinsic to the star, but the length of the time series is insufficient to clarify this statement. Therefore these two frequencies were neglected in the stellar modeling process.

5.1.2 Interpretation

The frequencies in the amplitude spectrum are separated into two groups (even perhaps into three considering the frequencies below 0.2 c/d). This pattern is consistent with Be-star behavior.

Be and SPBe stars

Be stars are stars which show one or more Balmer emission lines in their spectra. These emission lines can vanish and appear on time scales of days to decades and are very wide (Doppler Broadening) due to the very fast rotation (~ 300 km/s) of those stars.

SPBe stars, i.e. Be stars which show nonradial, high-order g-mode pulsations excited by the κ-mechanism (see Section 2.1.2), show grouping effects in their amplitude spectra: in the co-rotating frame of a rapidly rotating SPBe star, the rotation frequency is always higher than the pulsation frequencies. This characteristic causes a grouping effect of the pulsation frequencies in the observer's frame. The frequency groups are separated from each other by $\approx |m|\Omega$, where m denotes the azimuthal order and Ω the rotation frequency. (Cameron et al. 2008).

In the following model (see Fig.5.23), excited frequencies of a $9M_{\odot}$ star are compared to the detected frequencies. The rotation frequency is assumed to be 1.12 c/d so that the frequencies of excited g-modes with $m = -1$ and $m = -2$ are around the observed second and third frequency group, respectively. The rotation frequency is nearly critical, which is consistent with the Be phenomena. The surface gravity of the model ($\log g = 3.754$) is slightly smaller than the one found with Geneva photometry ($\log g = 4.07 \pm 0.16$). Probably the calibration method by Kunzli et al. (1997) is not appropriate for peculiar and emission line stars. The effective temperature however, is basically the same as the one found with Geneva photometry. Although this new value for the surface gravity shifts the star upwards in the $\log g$-$\log T$ diagram, HD 259481 still remains in the instability strip of SPB stars.

frequency [c/d]	amp [mmag]	sig	S/N	O/SL	cind	disc	model
1.535 ± 0.002	5.53	805.89	48.61				X
0.057 ± 0.003	3.09	304.12	29.86			X	
0.103 ± 0.003	2.14	199.27	24.17			X	
2.734 ± 0.003	1.96	191.62	23.70				X
2.536 ± 0.004	1.86	177.52	22.81				X
0.190 ± 0.004	1.62	145.74	20.67		X		
2.829 ± 0.004	1.51	133.01	19.75				X
0.267 ± 0.005	1.32	109.87	17.95				X
1.361 ± 0.005	1.23	97.84	16.94				X
0.354 ± 0.005	1.12	83.54	15.65				X
1.019 ± 0.005	1.08	81.54	15.46				X
2.694 ± 0.007	0.82	48.20	11.89				X
17.191 ± 0.008	0.73	38.99	10.69	X			
0.221 ± 0.008	0.67	33.51	9.91				X
12.189 ± 0.008	0.66	32.65	9.78	X			
1.194 ± 0.009	0.64	31.06	9.54		X		
1.151 ± 0.009	0.63	30.69	9.49				X
1.579 ± 0.009	0.59	26.77	8.86				X
3.065 ± 0.009	0.58	26.31	8.78				X
16.189 ± 0.010	0.55	23.50	8.30	X			
2.899 ± 0.011	0.50	20.05	7.67				X
1.294 ± 0.011	0.50	19.80	7.62				X
2.607 ± 0.011	0.46	17.43	7.15				X
0.896 ± 0.012	0.43	15.47	6.73				X
2.441 ± 0.012	0.44	15.71	6.79				X
1.408 ± 0.013	0.41	13.76	6.35				X

Table 5.2: SigSpec frequencies of HD 259481 with Kallinger errors, amplitudes (amp), significances (sig), signal-to-noise ratios (S/N). The ‘X’ in the following columns indicates if the frequency is an orbit or a side-lobe (O/SL), if it was found in the comparison data set using Cinderella (cind), if it was discarded (disc) or if it was used for stellar modelling (model).

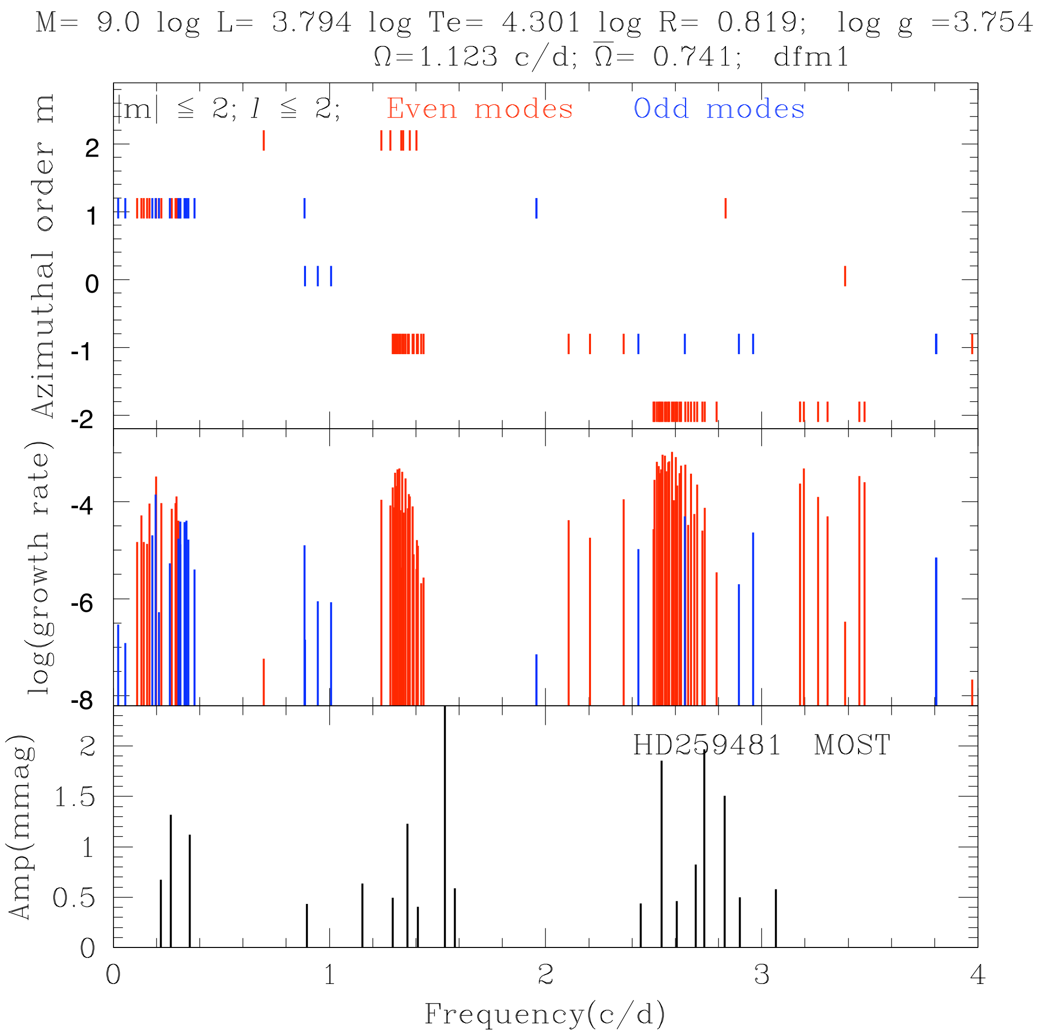

Figure 5.4: Model of HD 259481 kindly provided by Hideyuki Saio (private communication).

5.2 GSC 00154-00785

GSC 00154-00785 is a $10^{\mathrm{m}}\!.9$, B9V star and was used as the 35th guide star in the NGC 2244 run. It is referred to as a 'Star in Cluster' in the SIMBAD astronomical data base and was observed for 21 days from December 28, 2007 to January 26, 2008. With a probability of 50% this star is a member of NGC 2244 (Chen et al. 2007).

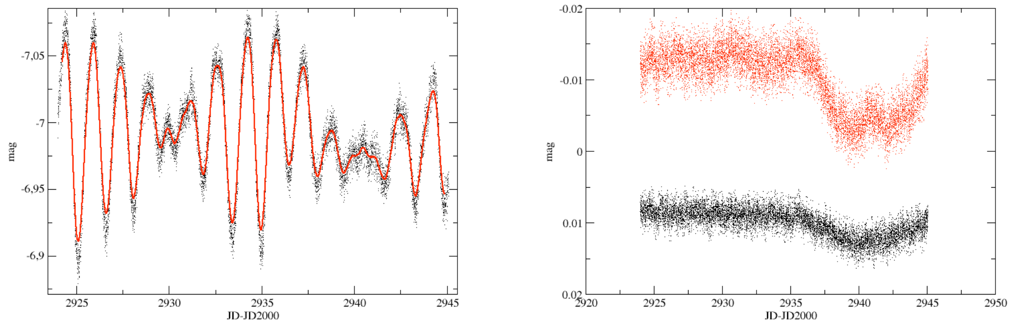

Figure 5.5: Left: light curve (black dots) and moving average (red line) of GSC 00154-00785 monitored by MOST for 21 days. Right: light curves of the comparison stars as shown in Fig. 5.2.

Using again SIGSPEC and CINDERELLA, the frequencies in table 5.3 are considered significant.

5.2.1 Interpretation

Assuming the spectral type B9V to be correct, Hideyuki Saio (private communication) managed to model these frequencies (see Fig.5.7).

This star seems to be a very slow rotator; the assumed rotation frequency is 0.22 c/d which corresponds to an equatorial velocity of $\sim$ 33–36km/s. The effective temperature is slightly higher than one would expect for a B9 star and corresponds rather to a B8 star.

Usually the frequency groupings observed in the amplitude spectrum are caused by fast rotation. But since the equatorial velocity is so low, it cannot contribute much to the groupings of GSC 00154-00785. They must have a different origin: it is shown here, for the first time, that frequency groupings can occur even for a slowly rotating star, given a relatively low effective temperature.

The coolest SPB star found so far is HD 121190 (Aerts & Kolenberg 2005) with $\log T_{\mathrm{eff}} = 4.082$. If the value for the effective temperature of GSC 00154-00785, $\log T_{\mathrm{eff}} = 4.08$, can be confirmed by other means, it will take HD 121190's place by a temperature difference of 50K. Contrary to GSC 00154-00785, HD 121190 rotates at much faster with $v \sin i = 118$km/s, i.e. 26% of its critical velocity.

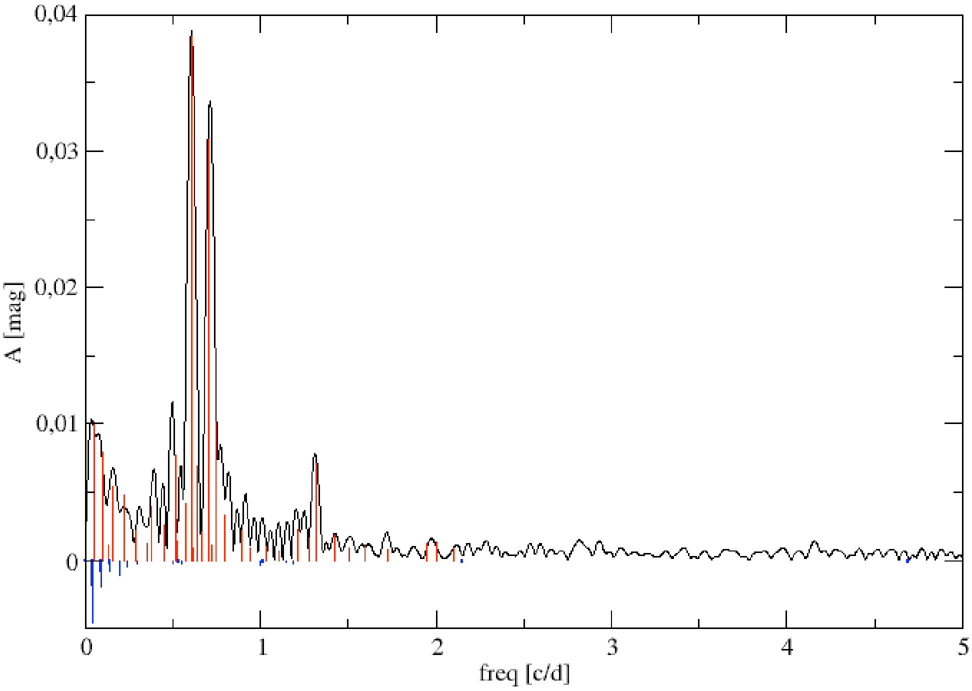

Figure 5.6: Region of interest of the amplitude spectrum of HD 259481 (black) with the identified frequencies (red) and identified frequencies of the two comparison stars HD 259480 and HD 46202 (violet and blue, respectively). For better visibility, the inverted amplitude axis is used to display the comparison star amplitudes.

frequency [c/d]	amp [mmag]	sig	S/N	O/SL	cind	disc	model
0.605 ± 0.001	38.44	1017.94	54.63				X
0.706 ± 0.001	30.85	1255.02	60.66				X
0.745 ± 0.003	10.19	339.08	31.53				X
0.050 ± 0.003	10.10	361.61	32.56		X		
0.101 ± 0.003	7.93	286.21	28.97		X		
0.516 ± 0.003	7.75	316.35	30.45				X
1.319 ± 0.003	7.10	311.16	30.20				X
0.641 ± 0.003	6.84	361.30	32.55				X
0.158 ± 0.003	5.40	244.46	26.77		X		
0.220 ± 0.003	4.75	205.49	24.54		X		
0.576 ± 0.003	4.15	188.76	23.52				X
0.379 ± 0.004	3.92	167.68	22.17				X
0.792 ± 0.004	3.28	121.16	18.85				X
0.453 ± 0.005	2.63	106.41	17.66				X
1.208 ± 0.006	2.27	72.89	14.62				X
0.890 ± 0.006	2.17	69.11	14.23				X
0.289 ± 0.006	2.14	61.86	13.47		X		
1.423 ± 0.006	1.89	61.16	13.39				X
0.665 ± 0.006	2.02	60.44	13.31				X
1.276 ± 0.007	1.65	46.41	11.66				X
0.522 ± 0.008	1.40	38.66	10.65		X		
0.350 ± 0.008	1.20	31.80	9.65				X
2.002 ± 0.009	1.32	27.51	8.98				X
1.942 ± 0.010	1.20	24.06	8.40				X
0.722 ± 0.010	1.13	24.34	8.45				X
0.133 ± 0.010	1.14	24.64	8.50		X		
1.592 ± 0.010	1.07	22.47	8.12				X
1.030 ± 0.011	0.98	18.33	7.33		X		
0.613 ± 0.011	0.95	17.74	7.21				X
0.944 ± 0.012	0.88	15.17	6.67				X
1.508 ± 0.012	0.88	14.96	6.62				X
2.103 ± 0.012	0.86	14.77	6.58				X
1.722 ± 0.014	0.77	11.90	5.91				X
1.105 ± 0.014	0.74	11.19	5.73				X

Table 5.3: SigSpec frequencies of GSC 00154-00785 with Kallinger errors, amplitudes (amp), significances (sig), signal-to-noise ratios (S/N). The 'X' in the following columns indicates if the frequency is an orbit or a side-lobe (O/SL), if it was found in the comparison data set using Cinderella (cind), if it was discarded (disc) or if it was used for stellar modelling (model).

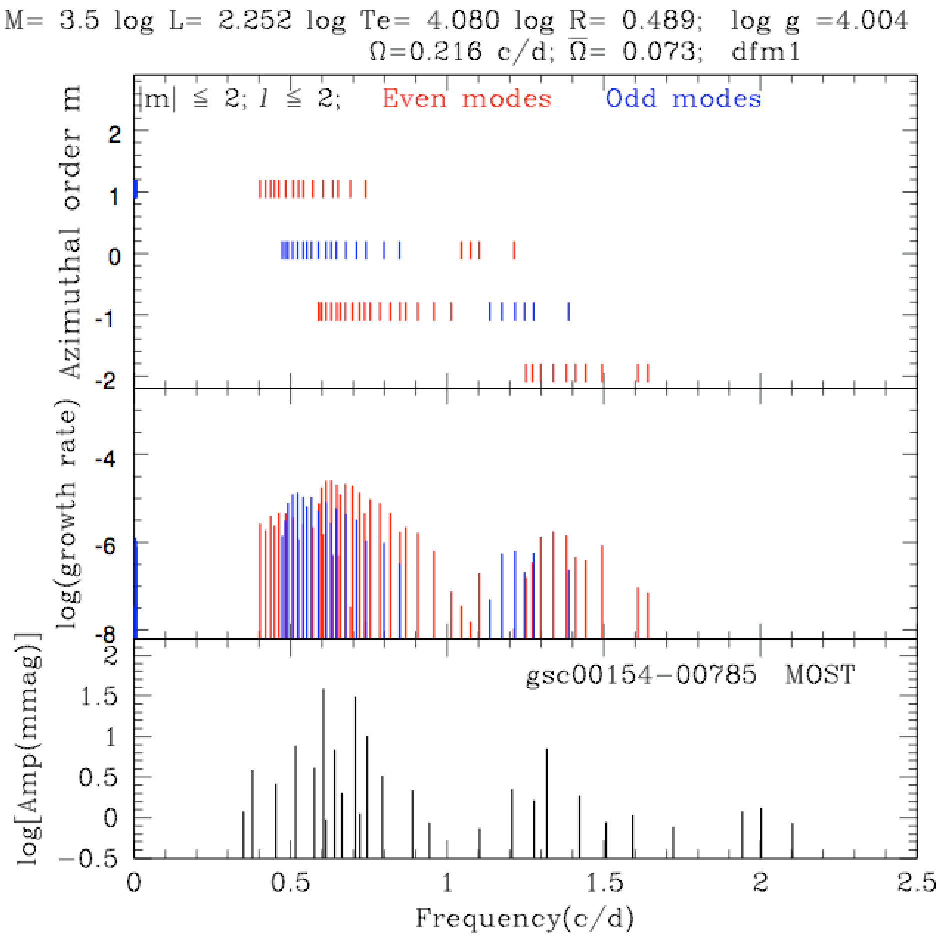

Figure 5.7: model of GSC 00154-00785. Notice the two frequency groupings around 0.7 c/d and 1.3 c/d

5.3 GSC 00154-01871

GSC 00154-01871 was the 36th guide star in the NGC 2244 run. This star has a visual magnitude of $10^{\mathrm{m}}\!.6$, is classified as B5 star in the SIMBAD astronomical data base and was observed from December 28, 2007 to January 26, 2008 for 21 days.

Chen et al. (2007) confirm the cluster membership with a probability of 84%. Spectroscopic measurments (Huang & Gies 2006) yield $T_{\rm eff} = 13605 \pm 59\,\mathrm{K}$ and $\log g = 3.797 \pm 0.012$.

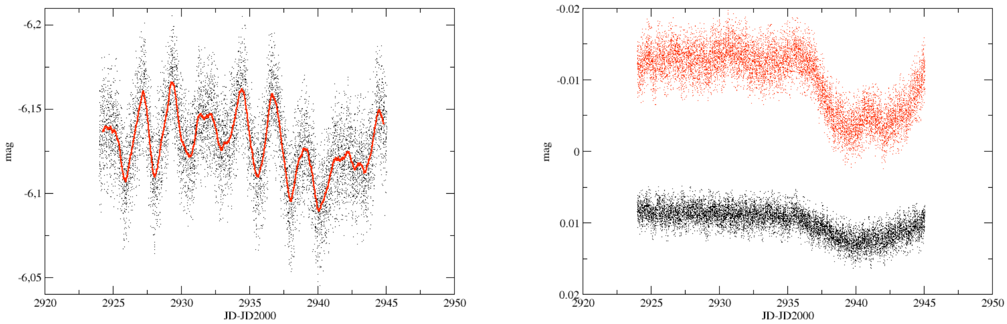

Figure 5.8: Left: light curve (black dots) and moving average (red line) of GSC 00154-01871 monitored by MOST for 21 days. Right: light curves of the comparison stars as shown in Fig. 5.2.

frequency [c/d]	amp [mmag]	sig	S/N	O/SL	cind	disc	model
0.406 ± 0.002	17.51	521.02	39.08				X
0.053 ± 0.002	14.15	415.42	34.90			X	
0.513 ± 0.002	8.16	201.98	24.33				X
0.102 ± 0.003	5.89	105.15	17.56			X	
0.460 ± 0.006	3.34	34.21	10.01				X
0.230 ± 0.006	2.83	34.09	10.00		X		
1.000 ± 0.006	2.90	30.49	9.45		X		
0.149 ± 0.007	2.47	21.38	7.92		X		
2.001 ± 0.008	2.17	16.97	7.05			X	
0.571 ± 0.010	1.88	12.78	6.12		X		
26.375 ± 0.010	1.75	11.13	5.71	X			
2.985 ± 0.011	1.69	10.61	5.58			X	

Table 5.4: SIGSPEC frequencies of GSC 00154-01871 with Kallinger errors, amplitudes (amp), significances (sig), signal-to-noise ratios (S/N). The 'X' in the following columns indicates if the frequency is an orbit or a side-lobe (O/SL), if it was found in the comparison data set using CINDERELLA (cind), if it was discarded (disc) or if it was used for stellar modelling (model).

5.3.1 Interpretation

The identified frequencies are listed in Table 5.4. The two frequencies 0.053 c/d and 0.102 c/d correspond to a period of 18.86 d and 9.8 d respectively. Even if the two frequencies could be intrinsic to the star, one would have to neglect both, because the time series is simply too short to

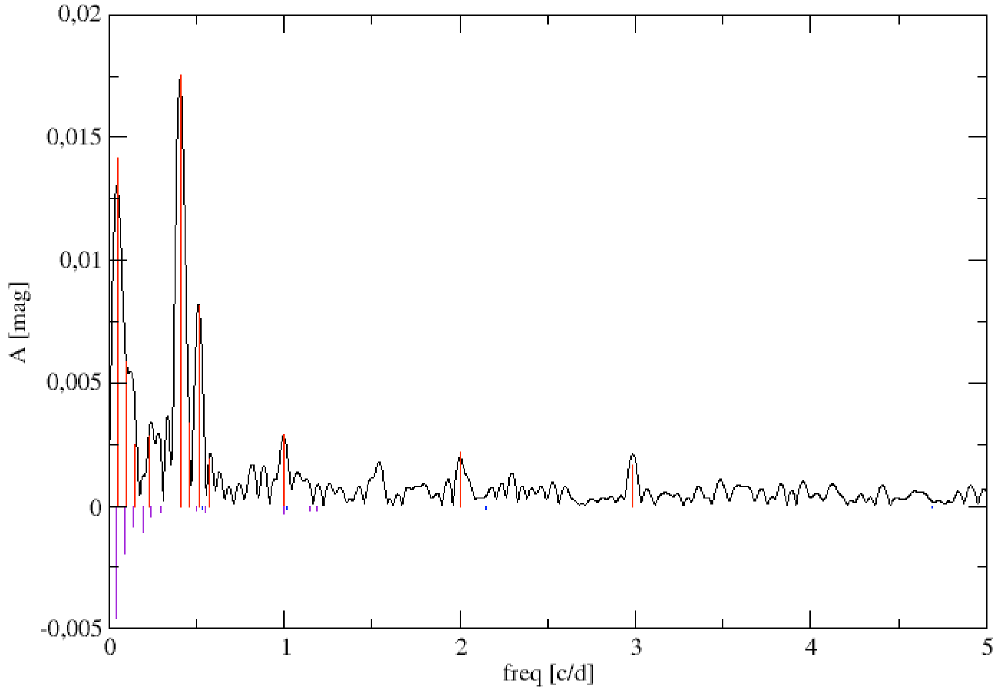

Figure 5.9: Region of interest of the amplitude spectrum of HD 259481 (black) with the identified frequencies (red) and identified frequencies of the two comparison stars HD 259480 and HD 46202 (violet and blue, respectively). For better visibility, the inverted amplitude axis is used to display the comparison star amplitudes.

confirm this. The frequencies at 2 c/d and 2.985 c/d are 1 c/d aliases, which is the known problem of the MOST satellite (see Section 5.1).

Using the parameters by Huang & Gies (2006) and assuming a rotational frequency of 0.26 c/d or 0.43 c/d respectively (corresponding to an equatorial velocity of $\sim$ 60km/s, $\sim$ 100km/s), many g-modes are excited in the theoretical models (see Fig.5.10 and Fig.5.11). Actually the frequency range of theoretically excited modes is considerably wider than the detected one.

Also the effect of rotation on the pulsation modes is small, because the rotation rate is relatively slow. However, Huang & Gies (2006) find a $v \sin i$ = 3km/s which is approximately two orders of magnitude lower than the equatorial velocity obtained from theory. One can explain this discrepancy, if $i \sim 0°$, i.e. one is looking at the star nearly pole-on. This in turn means, only axis-symmetric modes, i.e. $m = 0$, can be detected, because cancellation occurs for the other cases. In particular, $l = 1$ modes (the blue lines at $m = 0$ in Fig.5.10 and Fig.5.11) should be most visible. Therefore the frequencies between $\sim$ 0.4 c/d and $\sim$ 0.5 c/d should be g-modes with $(m, l) = (0, 1)$.

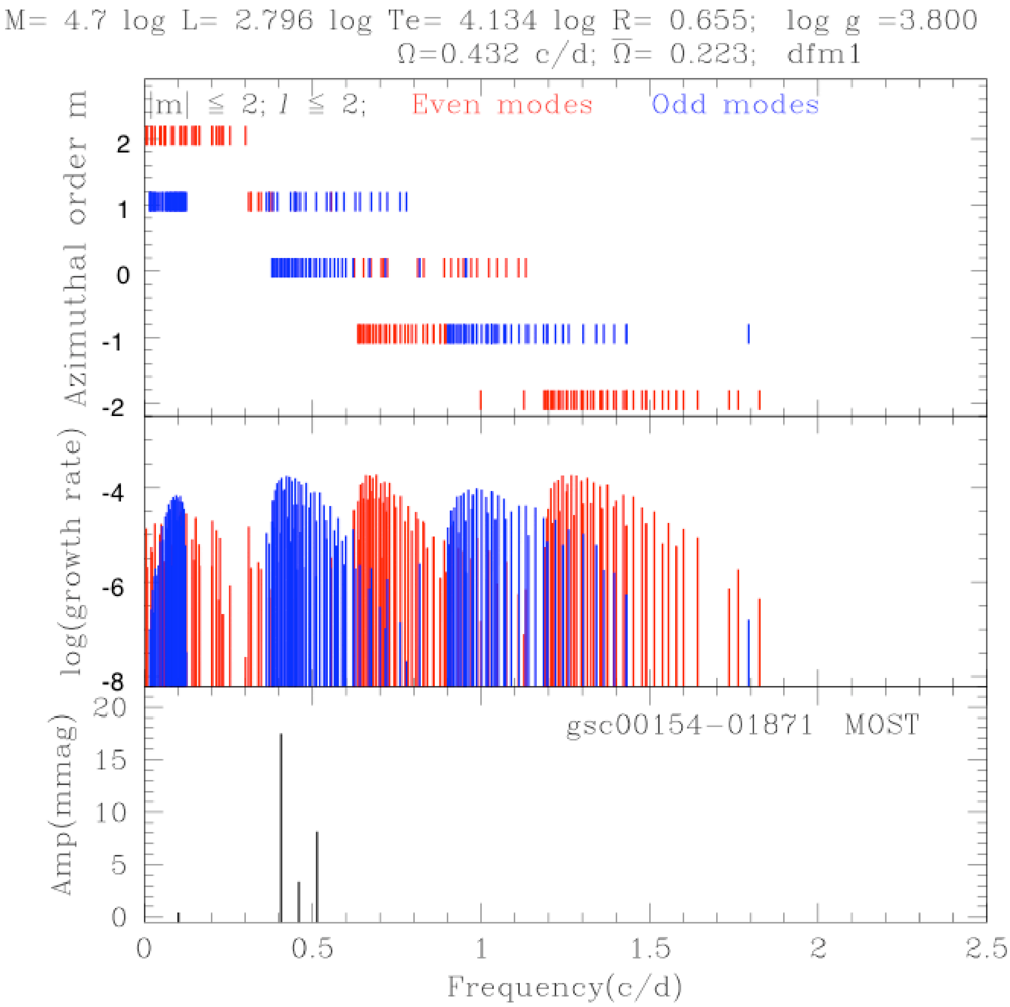

Figure 5.10: model of GSC 00154-01871 with $\Omega = 0.432\,\mathrm{c/d}$ (kindly provided by Hideyuki Saio; private communication).

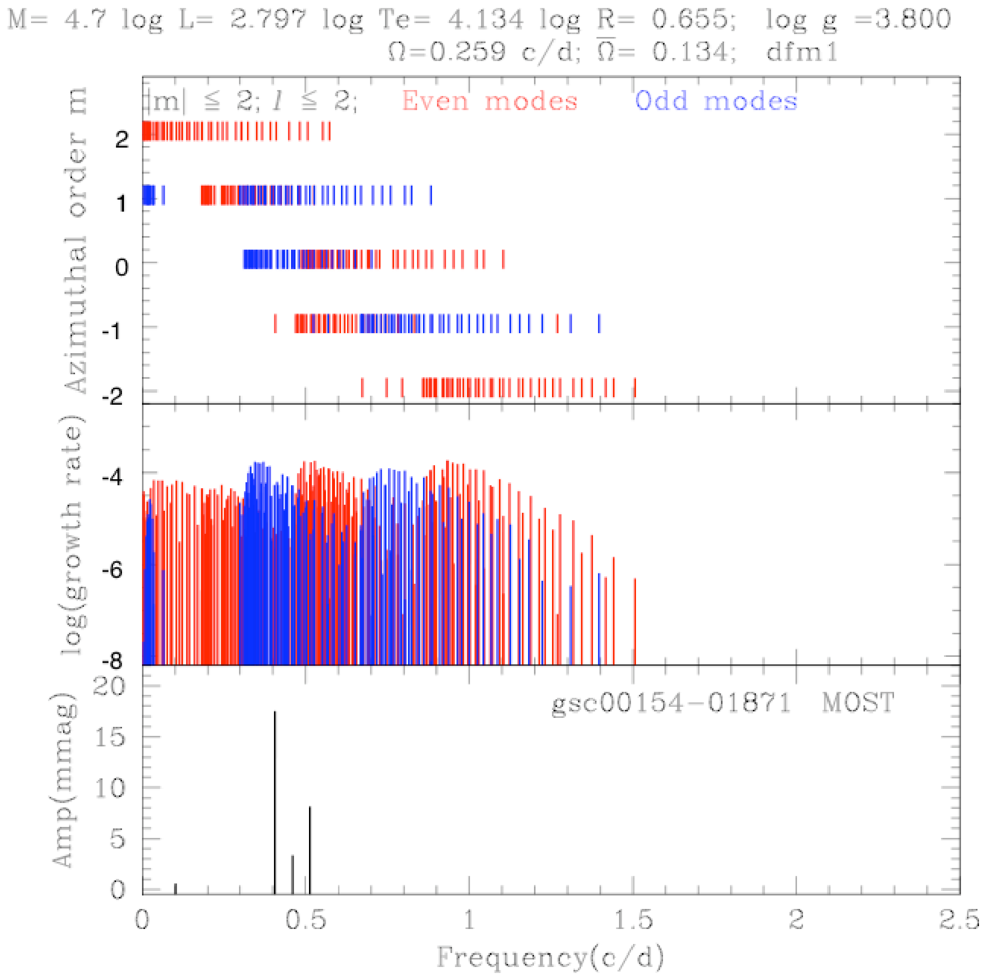

Figure 5.11: model of GSC 00154-01871 with $\Omega = 0.259\,c/d$ (kindly provided by Hideyuki Saio; private communication).

5.4 GSC 00750-01778

GSC 00750-01778 (HD 261810), the 21$^{\text{th}}$ guide star in the second NGC 2264 run, is identified as star nr. 88[2] in the young open cluster NGC 2264. The star is a member of this cluster with a probability of 74% (Vasilevskis et al. 1965). It has a visual magnitude of $9\overset{\text{m}}{.}15$ and is classified as a B1, optically detected pre-main sequence star in the SIMBAD astronomical database. HD 261810 was monitored for approximately 24 days by the MOST satellite from December 7, 2006, to January 1, 2007.

For this star a lot of measurements are avaiable on SIMBAD. UBV measurements (Shulov et al. (1983)) and Geneva photometry (Rufener 1976) are available. (U: 0.636, V: 1.065, $B1$: 0.813, $B2$: 1.547, $V1$: 1.747, G: 2.257). Again "calib.f" was used to determine the effective temperature $T_{\text{eff}} = 16862 \pm 311\,\text{K}$ and the surface gravity $\log g = 4.52 \pm 0.22$. Fortunately also Strømgren photometry ($b-y = -0.039 \pm 0.003$, $m1 = 0.081 \pm 0.003$, $c1 = 0.303 \pm 0.007$) and Hβ line measurement ($H\beta = 2.696 \pm 0.00$) are available (Hauck & Mermilliod 1998). This can be used as well to derive the fundamental parameters. Using the calibration method by Napiwotzki et al. (1993), we obtain $T_{\text{eff}} = 17282 \pm 146\,\text{K}$ and $\log g = 4.37 \pm 0.09$. These values are in perfect agreement with the ones obtained from the Geneva photometry (see Fig.5).

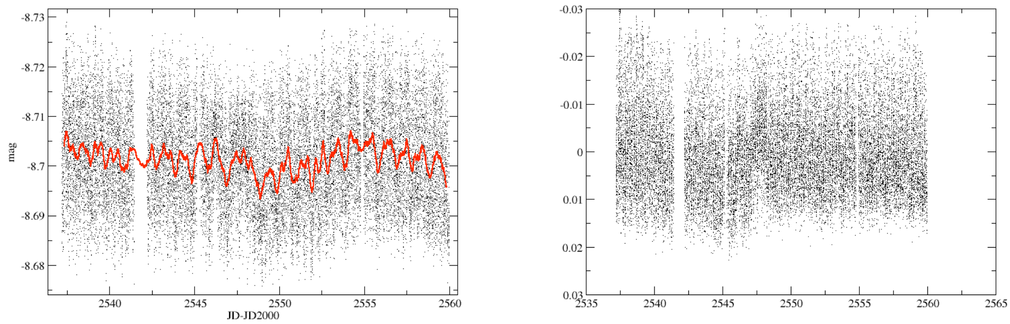

Figure 5.12: Left: light curve (black dots) and moving average (red line) of HD 261810 monitored by MOST for 23 days. Right: light curves of the comparison star HD 261736.

5.4.1 Comparison star

The comparison data sets for CINDERELLA were the stars from the same observation run of NGC 2244 (HD 261878, HD 47469) and the constant star HD 261736 identified as star 46 in NGC 2264 (Walker 1956), classified as an A3IV in the SIMBAD astronomical data base (α: $6^h\,40^m\,24.748^s$ and $\delta = 9^\circ\,46'\,08.41''$).

5.4.2 Interpretation

Averaging the fundamental parameters derived from Geneva photometry ($\log T_{\text{eff}} = 4.227 \pm 0.009$ and $\log g = 4.52 \pm 0.22$) and Strømgren photometry ($\log T_{\text{eff}} = 4.238 \pm 0.004$ and $\log g = 4.37 \pm 0.09$)

[2]according to the numbering system by Walker (1956)

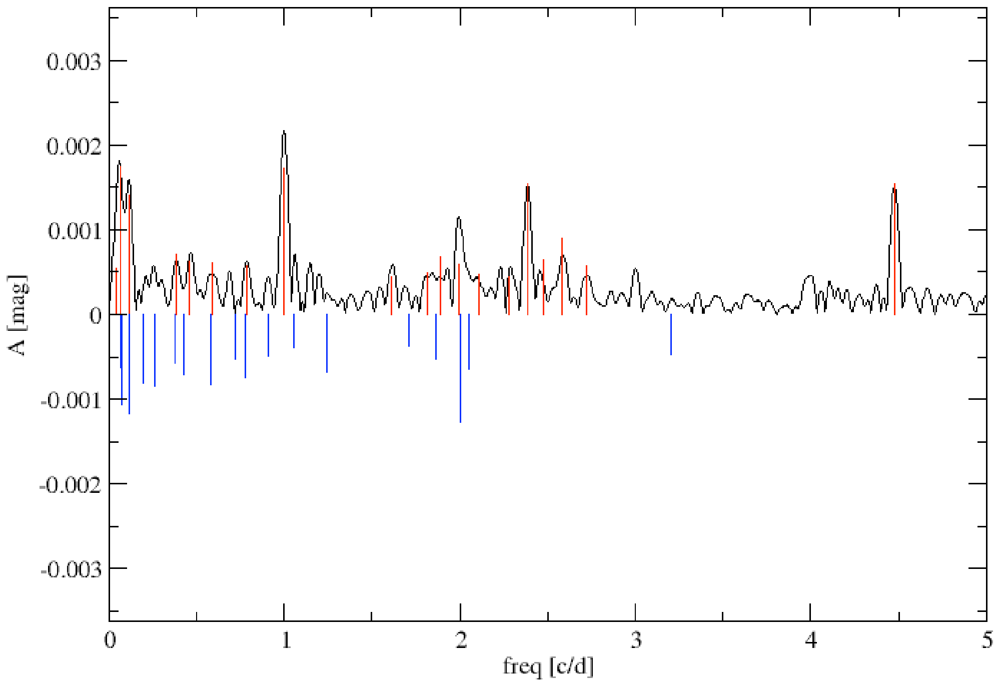

Figure 5.13: Region of interest of the amplitude spectrum of HD 261810 (black) with the identified frequencies (red) and identified frequencies of the comparison star HD 261736 (blue). For better visibility, the inverted amplitude axis is used to display the comparison star amplitudes.

frequency [c/d]	amp [mmag]	sig	S/N	O/SL	cind	disc	model
14.198 ± 0.002	7.82	467.59	37.0	X			
1.000 ± 0.004	1.72	106.12	17.6		X		
0.069 ± 0.005	1.75	87.99	16.1		X		
4.478 ± 0.005	1.55	81.22	15.4				X
0.116 ± 0.005	1.40	71.13	14.4		X		
2.388 ± 0.005	1.54	64.38	13.7				X
1.997 ± 0.007	0.60	34.73	10.1		X		
2.582 ± 0.009	0.89	21.38	7.9				X
26.381 ± 0.011	0.91	16.70	7.0	X			
0.386 ± 0.011	0.71	14.61	6.5		X		
0.457 ± 0.012	0.62	14.33	6.5				X
1.889 ± 0.012	0.69	12.61	6.1		X		
2.481 ± 0.012	0.64	13.02	6.2				X
11.203 ± 0.012	0.65	12.76	6.1	X			
0.593 ± 0.013	0.60	12.24	6.0		X		
16.207 ± 0.013	0.83	12.08	5.9	X			
0.788 ± 0.013	0.57	12.20	6.0		X		
2.721 ± 0.014	0.57	10.55	5.6				X
0.042 ± 0.014	0.55	10.19	5.5		X		
14.446 ± 0.014	0.55	9.57	5.3	X			
27.399 ± 0.014	0.55	9.45	5.3	X			
7.209 ± 0.015	0.50	8.86	5.1			X	
18.186 ± 0.015	0.49	8.83	5.1	X			
27.352 ± 0.016	0.48	7.96	4.8	X			
2.109 ± 0.016	0.47	7.94	4.8				X
28.301 ± 0.017	0.49	6.82	4.5	X			
28.346 ± 0.017	0.44	6.50	4.4	X			
1.814 ± 0.017	0.49	6.43	4.3				X
1.610 ± 0.017	0.45	7.01	4.5				X
2.283 ± 0.017	0.44	6.35	4.3				X
9.520 ± 0.018	0.41	6.04	4.2			X	
17.186 ± 0.019	0.40	5.58	4.0	X			
14.503 ± 0.020	0.39	5.04	3.8	X			
13.118 ± 0.019	0.39	5.08	3.9	X			

Table 5.5: SigSpec frequencies of HD 261810 with Kallinger errors, amplitudes (amp), significances (sig), signal-to-noise ratios (S/N). The 'X' in the following columns indicates if the frequency is an orbit or a side-lobe (O/SL), if it was found in the comparison data set using Cinderella (cind), if it was discarded (disc) or if it was used for stellar modelling (model).

yields $\log T_{\rm eff} = 4.233 \pm 0.007$ and $\log g = 4.45 \pm 0.17$. These values are reproduced by a model very close to the ZAMS (Fig.5.14). A mass of $5M_\odot$ is consistent with the effective temperature. To match the frequency groups around 2.5 c/d and 4.5 c/d, a rotation frequency of 1.814 c/d is adopted, which is about half the critical rate. Although the frequencies of excited $m = -1$ g-modes agree with the observed ones, the range of the predicted modes is narrower than the detected one. This problem has to be solved yet. The retrograde odd modes with $m = 1$ around 0.5 c/d are r-modes, the visibility of which is probably low. The frequency at 4.5 c/d can be identified as a g-mode with $m = -2$.

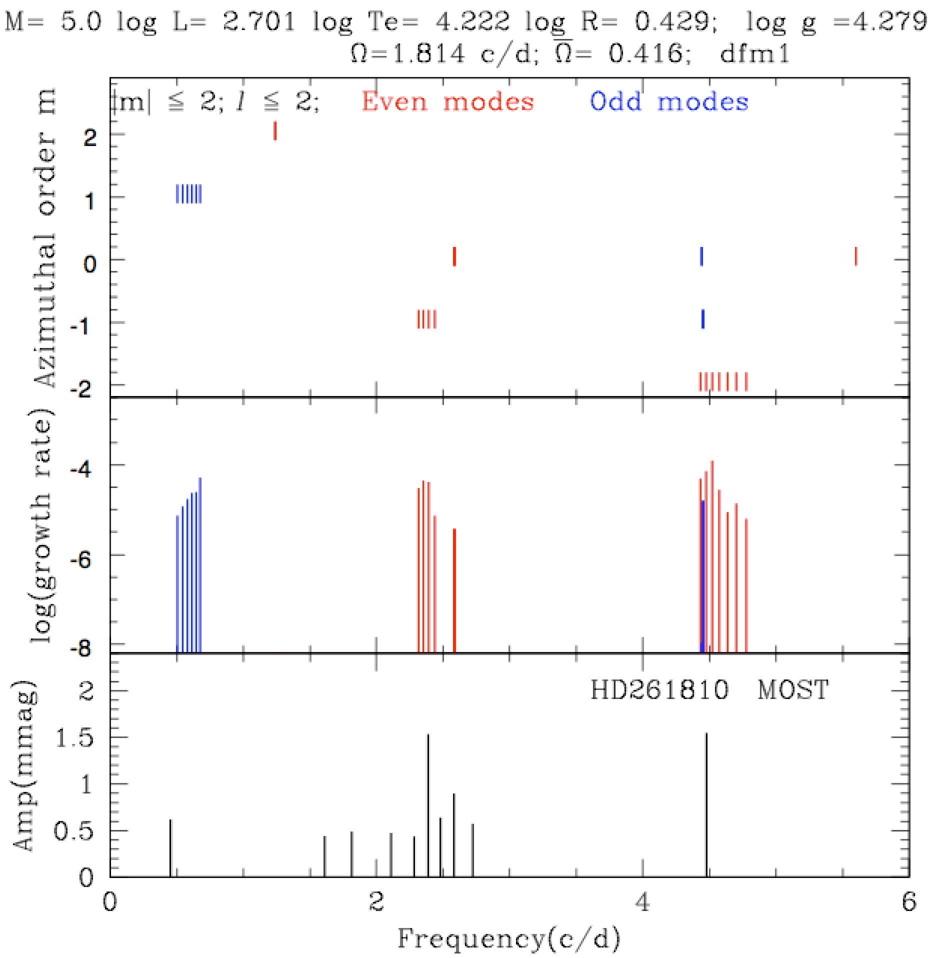

Figure 5.14: model of HD 261810 obtained with Geneva photometry, kindly provided by Hideyuki Saio (private communication).

5.5 GSC 00750-01876

GSC 00750-01876 (HD 261878), the 28^{th} guide star in the second NGC 2264 run, is identified as star nr. 109 in the young open cluster NGC 2264 and is a member with a probability of 94% (Vasilevskis et al. 1965). The star has a visual magnitude of $9^{\mathrm{m}}.18$ and is classified as an A0 star in the SIMBAD astronomical database. HD 261878 was monitored for approximately 23 days by the MOST satellite from December 7, 2006 to January 1, 2007.

For this star both Geneva (Burki et al. 1999) and Strømgren photometry (Hauck & Mermilliod 1998) is available. From Geneva photometry (U: 0.746, V: 1.096, $B1$: 0.823, $B2$: 1.545, $V1$: 1.783, G: 2.308), one obtains $T_{\mathrm{eff}} = 14692 \pm 101\,\mathrm{K}$ and $\log g = 4.64 \pm 0.11$. Strømgren photometry ($b - y = -0.044 \pm 0.011$, $m1 = 0.106 \pm 0.017$, $c1 = 0.386 \pm 0.003$), on the other hand, yields $T_{\mathrm{eff}} = 15462 \pm 414\,\mathrm{K}$ and $\log g = 4.45 \pm 0.08$. The two results agree perfectly.

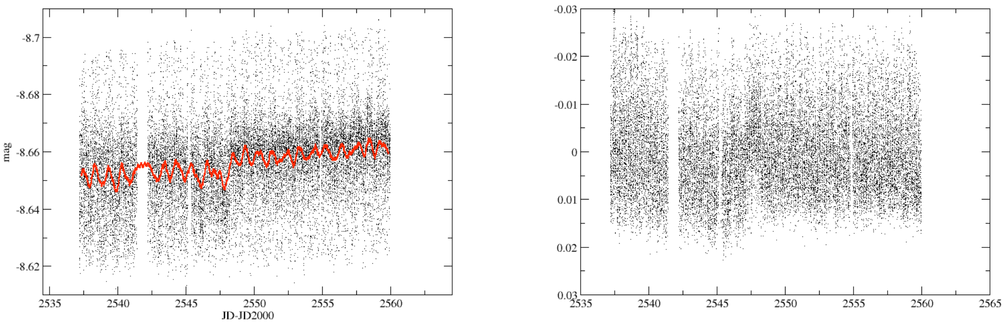

Figure 5.15: Left: light curve (black dots) and moving average (red line) of HD 261878 monitored by MOST for 23 days. Right: light curves of the comparison star HD 261736.

5.5.1 Comparison star

Also in this case, all stars from the same observation run (HD 261810, HD 47469) together with the constant star HD 261736 (already mentioned in Section 5.4) were used as comparison data sets for CINDERELLA.

Excluding those frequencies which are caused by the orbit, its side lobes and harmonics and those identified by CINDERELLA (both in the reference star and other target stars of the same observation run), one has also to reject the frequency of 0.025 c/d because it is too low compared to the total observation time of 22.77 days. The frequency of 1 c/d is the known MOST problem already mentioned above. Thus, only two frequencies are left.

5.5.2 Interpretation

With only two remaining frequencies, stellar modeling is senseless. The peak at 1.5 c/d could of course refer to a g-mode, but it is more likely to the rotational frequency of the star. The MOST measurements do not confirm HD 261878 to be a SPB star.

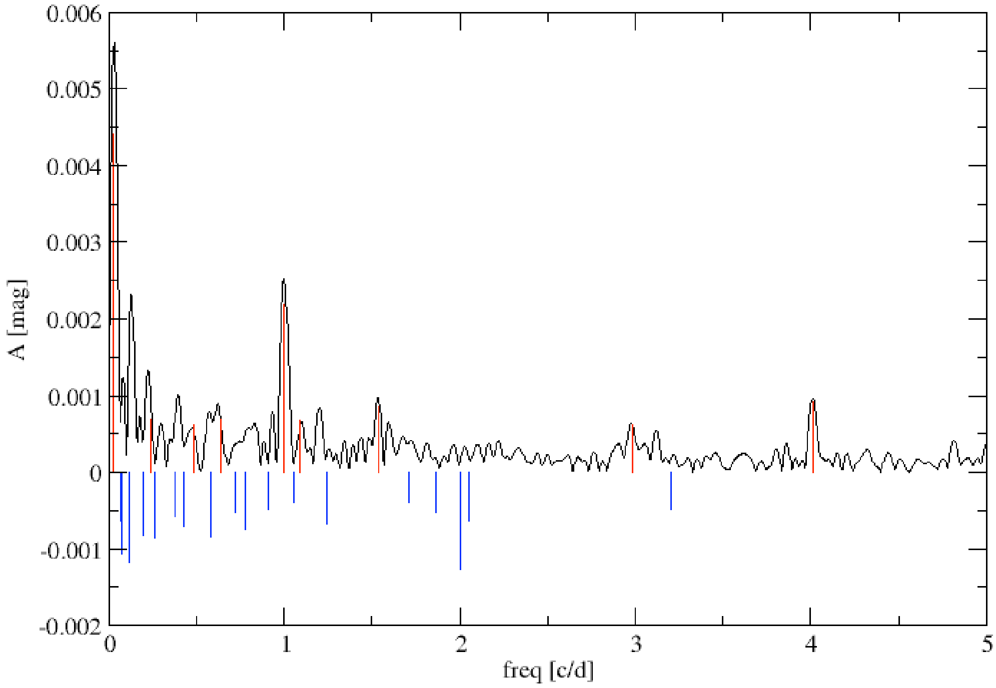

Figure 5.16: Region of interest of the amplitude spectrum of HD 261878 (black) with the identified frequencies (red). Identified frequencies of the comparison star HD 261736 are displayed in blue color. For better visibility, the inverted amplitude axis is used to display the comparison star amplitudes.

frequency [c/d]	amp [mmag]	sig	S/N	O/SL	cind	disc	model
0.025 ± 0.002	4.41	321.32	30.7			X	
28.382 ± 0.003	14.87	250.12	27.1	X			
1.001 ± 0.004	2.18	105.45	17.6			X	
14.194 ± 0.009	19.12	23.78	8.3	X			
28.397 ± 0.006	7.42	55.50	12.8	X			
28.365 ± 0.007	4.47	34.46	10.1	X			
28.327 ± 0.009	1.80	23.99	8.4	X			
14.096 ± 0.011	1.33	17.05	7.1	X			
1.535 ± 0.012	0.87	12.79	6.1				X
4.011 ± 0.013	0.93	12.00	5.9				X
14.019 ± 0.013	1.14	11.88	5.9	X			
28.422 ± 0.013	0.95	11.64	5.8	X			
0.239 ± 0.016	0.70	7.18	4.6		X		
12.990 ± 0.017	0.59	6.55	4.4	X			
27.401 ± 0.017	0.73	6.39	4.3	X			
28.577 ± 0.018	0.66	5.73	4.1	X			
1.088 ± 0.019	0.68	5.47	4.0		X		
16.182 ± 0.019	0.63	5.44	4.0	X			
0.635 ± 0.019	0.69	5.49	4.0		X		
2.981 ± 0.019	0.61	5.37	4.0		X		
0.485 ± 0.019	0.62	5.45	4.0		X		

Table 5.6: SigSpec frequencies of HD 261878 with Kallinger errors, amplitudes (amp), significances (sig), signal-to-noise ratios (S/N). The 'X' in the following columns indicates if the frequency is an orbit or a side-lobe (O/SL), if it was found in the comparison data set using Cinderella (cind), if it was discarded (disc) or if it was used for stellar modelling (model).

5.6 GSC 00750-01119

GSC 00750-01119 (HD 47469), the 4^{th} guide star in the second NGC 2264 run, is identified to star #7 in the young open cluster NGC 2264 (Walker 1956). However, no estimate of a membership probability could be found. The star has a visual magnitude of $7\overset{m}{.}8$ and is classified as a B5V star in the SIMBAD astronomical database. HD 47469 was monitored for approximately 23 days by the MOST satellite from December 7, 2006 to January 1, 2007.

For this star, Geneva (Rufener 1976) and Strømgren photometry, together with a $H\beta$ line measurement (Pena et al. 2000) is available. From Geneva photometry (U: 0.660, V: 1.096, $B1$: 0.802, $B2$: 1.554, $V1$: 1.782, G: 2.302) one gets $T_{\text{eff}} = 16075 \pm 138\,\text{K}$ and $\log g = 4.37 \pm 0.13$. Strømgren photometry ($b - y = -0.037$, $m1 = 0.105$, $c1 = 0.373$) delivers however a completely different result: $T_{\text{eff}} = 15608$ and $\log g = 3.87 \pm 0.07$. Although the temperature differs by only about 500 K the surface gravity from Strømgren photometry is considerably smaller.

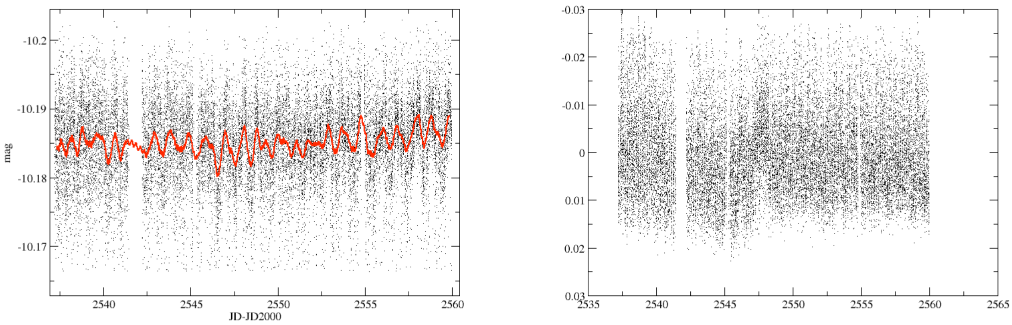

Figure 5.17: Left: light curve (black dots) and moving average (red line) of HD47469 monitored by MOST for 23 days. Right: light curves of the comparison star HD 261736.

5.6.1 Comparison star

The stars HD 261810 (Section 5.4) and HD 261878 (Section 5.5), together with the constant star HD 261736 (Section 5.4 and Section 5.5) were used as comparison data sets in CINDERELLA.

5.6.2 Interpretation

As mentioned above, although the estimates for the effective temperature are essentially identical, the surface gravity differs considerably, between Strømgren ($\log g = 3.87$) and Geneva photometry ($\log g = 4.37 \pm 0.13$). Therefore two different models were calculated by Hideyuki Saio (private communication).

Modeling with Geneva parameters: $\log T_{\text{eff}} = 4.206 \pm 0.004$ **and** $\log g = 4.37 \pm 0.13$

These values are reproduced by a $4.5 M_{\odot}$ ZAMS model (Fig.5.19). To match the frequency group around 2.9 c/d the rotational frequency 0.861 c/d is adopted. Because of the high $\log g$ value, the

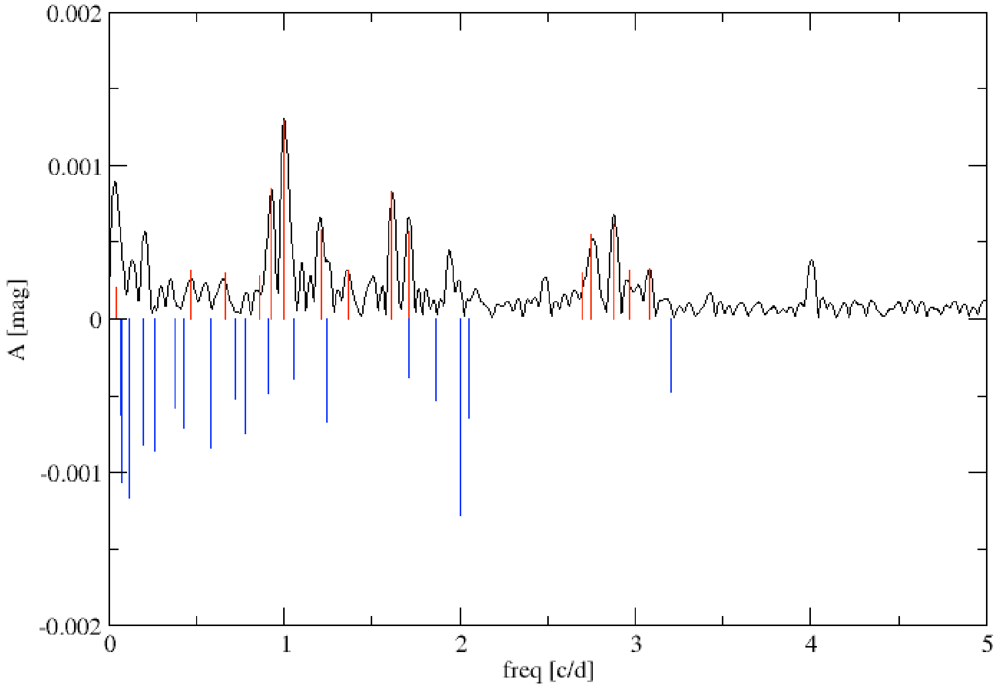

Figure 5.18: Region of interest of the amplitude spectrum of HD 47469 (black) with the identified frequencies (red) and identified frequencies of the comparison star HD 261736 (blue). For better visibility, the inverted amplitude axis is used to display the comparison star amplitudes.

frequency [c/d]	amp [mmag]	sig	S/N	O/SL	cind	disc	model
28.387 ± 0.002	5.60	316.92	30.48	X			
1.000 ± 0.004	1.29	137.96	20.11		X		
14.174 ± 0.005	4.84	79.69	15.28	X			
1.615 ± 0.006	0.83	60.84	13.36				X
29.386 ± 0.006	0.70	48.46	11.92	X			
28.397 ± 0.006	3.47	52.13	12.36	X			
0.924 ± 0.006	0.85	51.50	12.29		X		
0.039 ± 0.007	0.20	39.19	10.72		X		
28.352 ± 0.007	1.78	42.54	11.17	X			
2.879 ± 0.008	0.61	29.57	9.31				X
14.210 ± 0.008	3.39	27.44	8.97	X			
1.209 ± 0.009	0.58	26.11	8.75				X
1.706 ± 0.009	0.57	26.43	8.80		X		
28.364 ± 0.009	0.77	25.86	8.71	X			
2.750 ± 0.010	0.55	20.26	7.71				X
0.210 ± 0.011	0.47	17.19	7.10		X		
12.238 ± 0.012	0.39	13.06	6.19	X			
27.386 ± 0.014	0.37	10.45	5.54	X			
1.363 ± 0.014	0.32	10.24	5.48				X
18.199 ± 0.014	0.35	10.29	5.49	X			
28.431 ± 0.014	0.41	10.41	5.53	X			
0.471 ± 0.015	0.32	8.59	5.02				X
15.239 ± 0.016	0.29	7.97	4.84	X			
3.081 ± 0.016	0.33	7.93	4.82				X
14.195 ± 0.015	1.41	9.05	5.15	X			
2.968 ± 0.015	0.32	8.52	5.00				X
2.695 ± 0.016	0.30	7.26	4.61		X		
0.660 ± 0.017	0.30	6.97	4.52		X		
0.861 ± 0.017	0.28	6.91	4.50				X
21.356 ± 0.018	0.26	5.95	4.18	X			
29.338 ± 0.019	0.24	5.19	3.90	X			

Table 5.7: SigSpec frequencies of HD 47469 with Kallinger errors, amplitudes (amp), significances (sig), signal-to-noise ratios (S/N). The 'X' in the following columns indicates if the frequency is an orbit or a side-lobe (O/SL), if it was found in the comparison data set using Cinderella (cind), if it was discarded (disc) or if it was used for stellar modelling (model).

radius of the star must be very small and therefore the adopted rotational frequency is very low compared to the critical rotational frequency ($\approx 0.7\sqrt{GM/R^3}$). Hence the theoretical frequencies of excited g-modes do not show clear groupings.

Modeling with Strømgren parameters: $\log T_{\rm eff} = 4.193$ **and** $\log g = 3.87$

For these parameters a considerably evolved $6M_\odot$ star is adopted. The rotational frequency is chosen in such a way that the frequency group around 2.9 c/d is matched: the star rotates at a frequency of 1.21 c/d which is considerably close ($\approx 84\%$) to the critical rate. This is similar to a Be star phenomena. The retrograde $m = 1$ odd modes in the range between 0.2 c/d and 0.4 c/d are r-modes, while the other excited modes are g-modes. Although the excited $m = -2$ g-modes cover the frequency range of the observed frequency group at 2.9 c/d, there are no theoretical modes to match the detected frequencies below 1.3 c/d (see Fig.5.20).

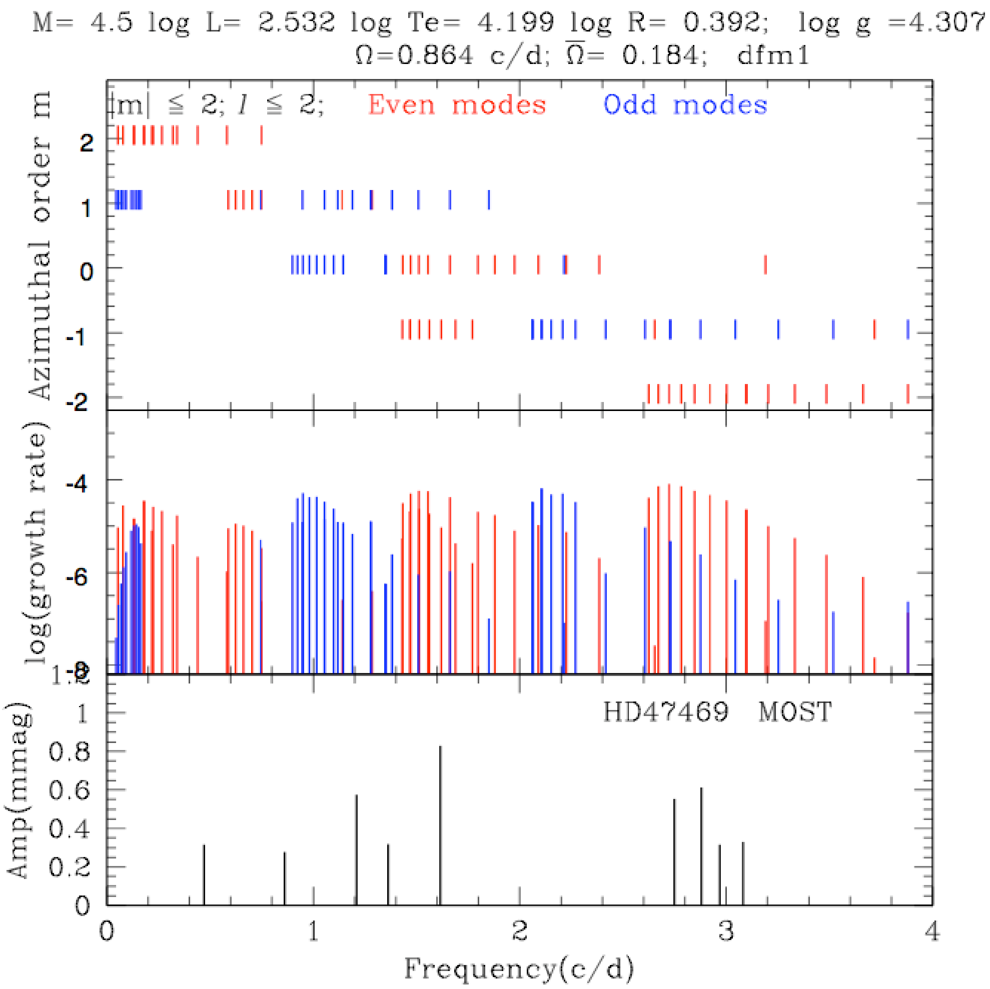

Figure 5.19: model obtained with Geneva photometry kindly provided by Hideyuki Saio (private communication).

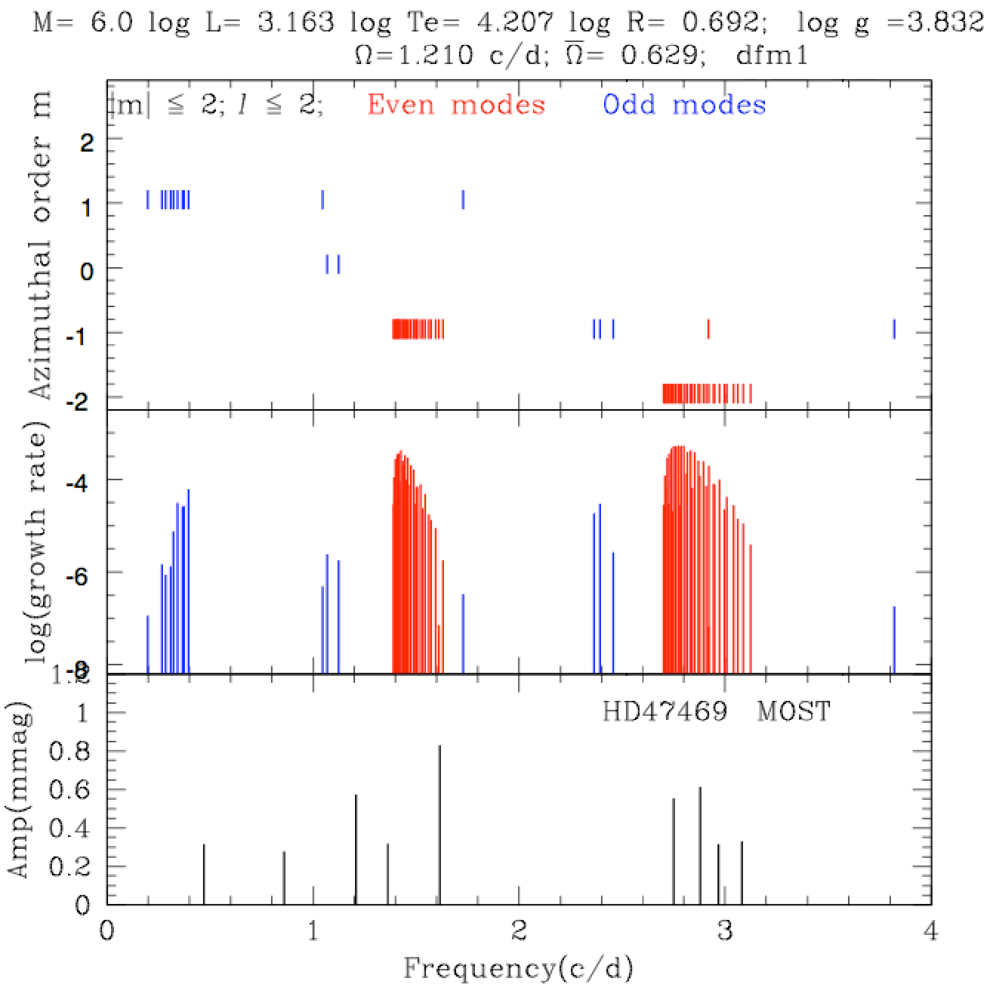

Figure 5.20: model obtained with Strømgren photometry kindly provided by Hideyuki Saio (private communication).

5.7 GSC 09007-02387

GSC 09007-02387 (HD 127696) is the 9$^{\text{th}}$ guide star in the α-Centauri run. The star has a visual magnitude of $9\overset{m}{.}1$ and is classified as a B7III/IV star in the SIMBAD astronomical database. Apparently HD 127696 is a star in a double system (Sinachopoulos 1988). HD 127696 was monitored for approximately 21 days by the MOST satellite from May 5, 2006 to June 6, 2006.

From Geneva photometry (U: 1.224 , V: 0.782 , $B1$: 0.870 , $B2$: 1.505 , $V1$: 1.489 , G: 1.918) (Burki et al. 1999) one gets $T_{\rm eff} = 12515 \pm 51\,\mathrm{K}$ and $\log g = 3.68 \pm 0.13$.

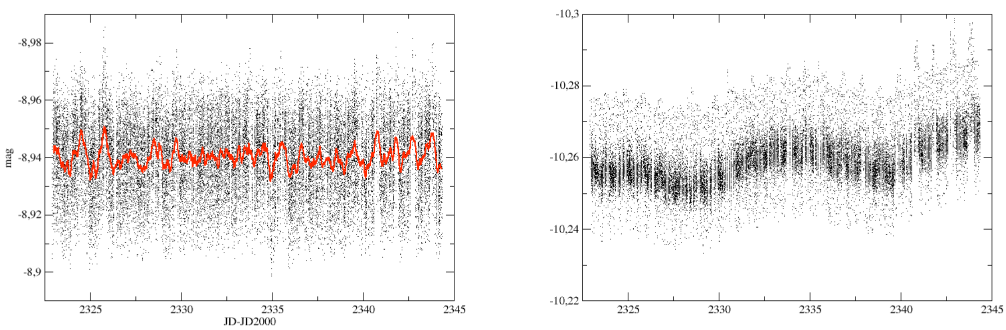

Figure 5.21: Left: Light curve of HD 127696 (black dots) with a moving average (red line) monitored over 31 days by MOST. Right: Light curve of the comparison star HD127755

5.7.1 Comparison star

The light curve of HD 127755 was chosen as comparison data set for CINDERELLA.

HD 127755 is classified as a K3III star in the SIMBAD astronomical data base (α: $14^h\,35^m\,29.82^s$ and δ: $-60^\circ\,38'\,30.91''$). The light curve is given in Fig. 5.21. There is obviously also some kind of intrinsic or instrumental variability present in the comparison data set (5 and 10 c/d).

The identified frequencies are listed in table 5.8. The four frequencies 0.954 c/d, 0.996 c/d, 2.082 c/d and 1.945 $^{-1}$ are very close to the 1 c/d, 2 c/d, respectively, and are therefore refuted.

5.7.2 Interpretation

The fundamental parameters obtained from Geneva photmetry are consistent with an evolved main sequence star of $4M_\odot$. The rotation rate is assumed to be 0.43 c/d in order to match the frequency group around 0.8 c/d with excited g-modes of $m = -1$. The rotation rate is approximately a quarter of the critical rate. However, this model is not in perfect agreement with the observed frequencies, because it cannot explain the frequencies higher than 2.4 c/d. So, from the most likely to the least likely case: either the observed frequencies are some artifacts not identified in the selection process, the calibrated effective temperature and surface gravity are wrong, the star is the first of a new class of variables or there is something wrong with physics.

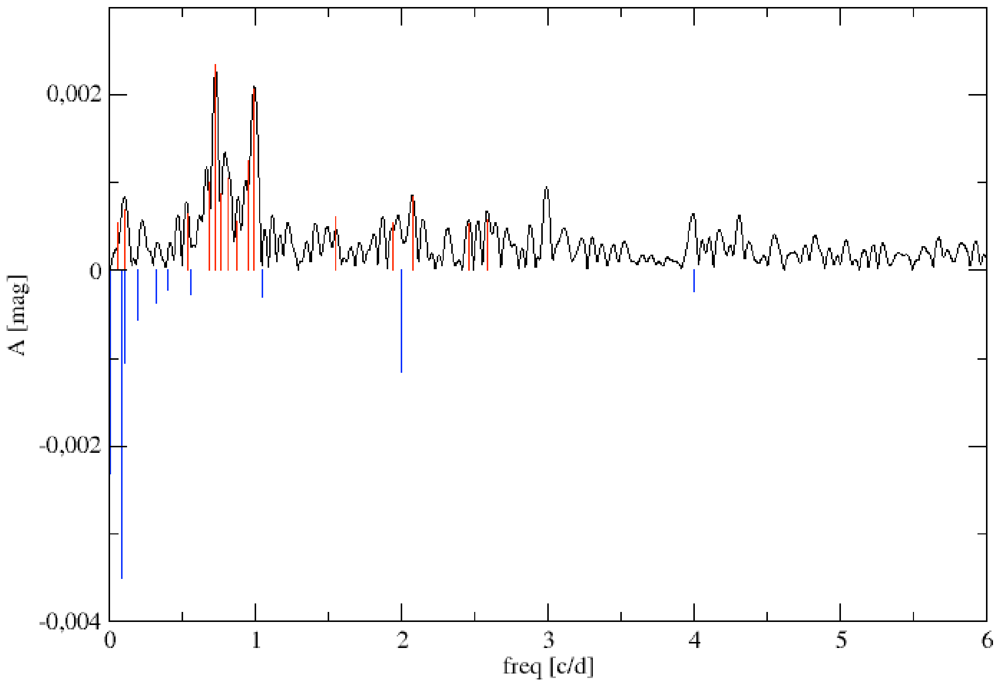

Figure 5.22: Region of interest of the amplitude spectrum of HD 127696 (black) with the identified frequencies (red) and identified frequencies of the comparison star HD 127755 (blue). For better visibility, the inverted amplitude axis is used to display the comparison star amplitudes.

frequency [c/d]	amp [mmag]	sig	S/N	O/SL	cind	disc	model
0.729 ± 0.005	2.34	103.73	17.44				X
0.996 ± 0.005	2.07	77.97	15.12			X	
27.397 ± 0.008	1.30	38.69	10.65	X			
14.196 ± 0.007	2.96	39.37	10.74	X			
17.189 ± 0.009	0.95	26.17	8.76	X			
0.817 ± 0.010	1.05	23.32	8.27				X
0.954 ± 0.011	1.25	19.17	7.50			X	
0.685 ± 0.011	1.00	19.47	7.55				X
0.768 ± 0.012	0.87	16.17	6.89				X
2.082 ± 0.013	0.84	13.95	6.40			X	
25.838 ± 0.013	0.65	12.59	6.08	X			
0.107 ± 0.014	0.70	10.87	5.65		X		
0.536 ± 0.015	0.65	10.36	5.51		X		
12.195 ± 0.015	0.77	10.20	5.47	X			
11.552 ± 0.016	0.65	8.47	4.98	X			
12.933 ± 0.017	0.59	7.83	4.79	X			
2.592 ± 0.017	0.58	7.71	4.76				X
23.829 ± 0.018	0.59	6.95	4.51	X			
1.550 ± 0.018	0.62	6.59	4.40				X
0.871 ± 0.019	0.55	6.27	4.29				X
29.462 ± 0.019	0.50	6.19	4.26	X			
2.460 ± 0.020	0.53	5.66	4.07				X
1.945 ± 0.020	0.55	5.39	3.97			X	
0.060 ± 0.020	0.55	5.62	4.06			X	

Table 5.8: SigSpec frequencies of HD 127697 with Kallinger errors, amplitudes (amp), significances (sig), signal-to-noise ratios (S/N). The 'X' in the following columns indicates if the frequency is an orbit or a side-lobe (O/SL), if it was found in the comparison data set using Cinderella (cind), if it was discarded (disc) or if it was used for stellar modelling (model).

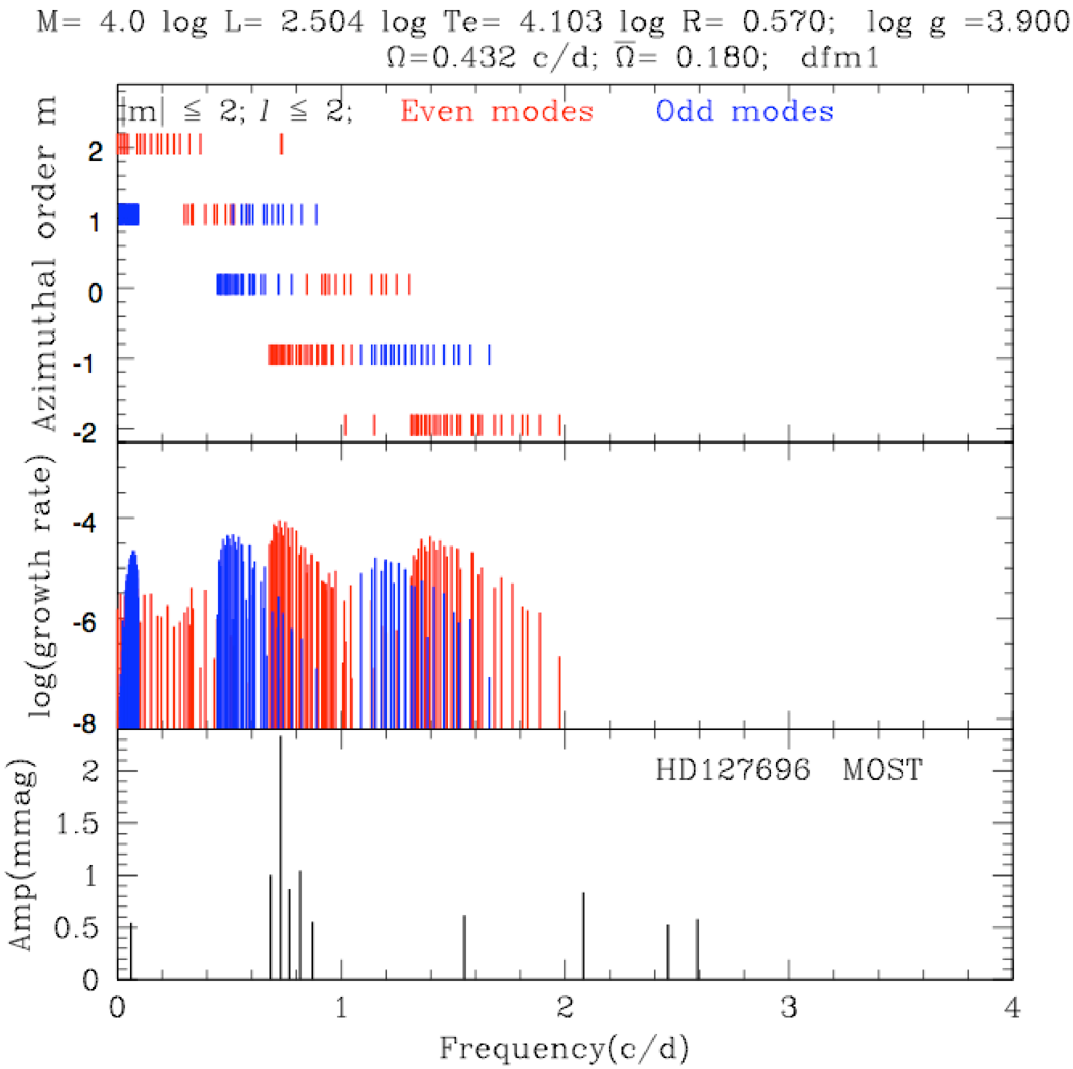

Figure 5.23: Model of HD 127696 kindly provided by Hideyuki Saio (private communication).

Chapter 6

Other guide stars

In this chapter, all those guide stars are listed, where neither T_{eff} nor $\log g$ could be estimated due to the lack of spectroscopic and multicolor photometric data or whose calibrated values were ambiguous. Sometimes, only the spectral type, which was available on SIMBAD, classified these stars as B stars. They are solely shown for completeness.

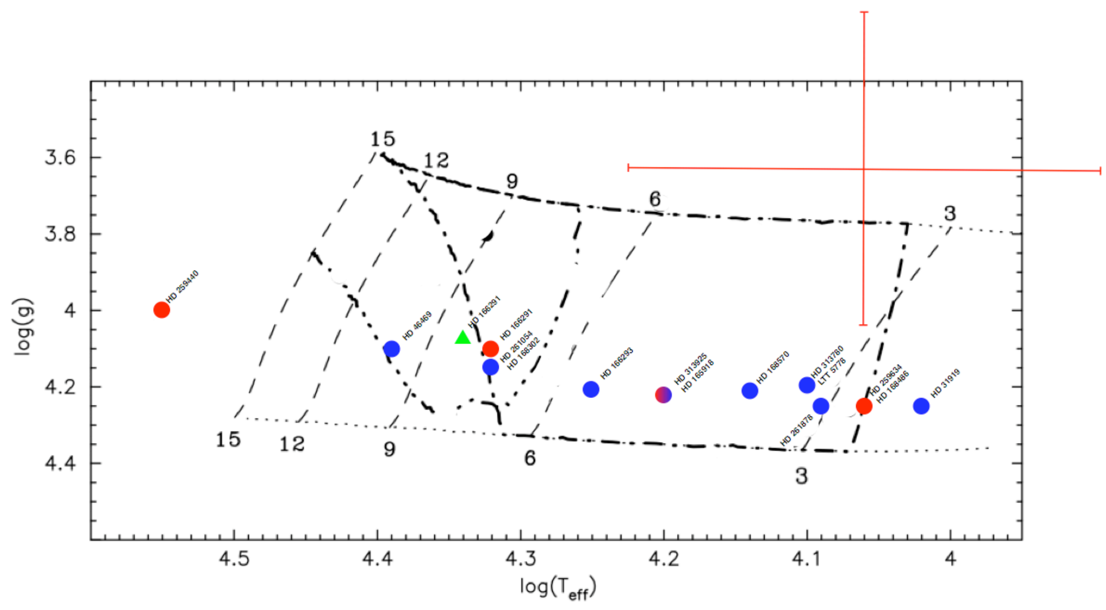

Figure 6.1: Position of all category-B (red) and -C (blue) stars in the $\log T_{\mathrm{eff}}$ and $\log g$ diagram. The fundamental parameters were deduced from the spectral- and luminosity class. The typical error bar is shown in the upper right corner

GSC identifier	other ID	spectral type	mag	RA [°]	DEC [°]
GSC 00158-03064	HD 259440	B0pe	9.12	6 32 59.25	5 48 01.18
GSC 06272-02378	HD 166291	B3II	8.88	18 10 38.24	-19 10 00.83
GSC 06276-01284	HD 313925	B5	10.6	18 09 01.72	-21 28 20.47
GSC 00154-02450	HD 259634	B9III	9.9	6 33 34.7	5 17 43
GSC 06265-01026	HD 168486	B9V	10.5	18 20 32.62	-16 19 18.43

Table 6.1: Category B stars: guide stars with unknown fundamental parameters but obvious signs of multiperiodicity.

GSC identifier	other ID	spectral type	mag	RA [°]	DEC [°]
GSC 00154-02287	HD 46469	B2V	8.55	6 33 48.73	5 28 49.52
GSC 00737-00304	HD 261054	B3e	9.75	06 38 09.17	09 29 05.24
GSC 06265-00615	HD 168302	B3III	9.17	18 19 39.41	-16 01 20.36
GSC 06276-02036	HD 166293	B3/B4III	8.26	18 10 47.12	-21 18 41.02
GSC 06272-01894	HD 165918	B5IV/V	8.17	18 09 04.64	-19 52 30.83
GSC 06265-01629	HD 168570	B7/B8Ib	10.51	18 21 05.92	-16 35 58.52
GSC 09007-04437	LTT5778	B8IV/V	8.59	14 37 38.74	-60 21 22.1
GSC 06276-02180	HD 313780	B8	10.03	18 08 50.4	-21 15 39.71
GSC 04741-00404	HD 31919	B9V	8.9	04 59 29.19	-2 03 59.57
GSC 00750-01876	HD 261878	A0-B5V	9.2	6 40 51.55	9 51 49.39
GSC 06265-00297	BD-16 4834	n.a.	9.63	18 21 27.81	-15 57 32.70

Table 6.2: Category C stars: guide stars with unknown fundamental parameters and bad light curves.

6.1 GSC 06272-02378

GSC 06272-02378 (HD 166291) was the 1st guide star in the field of WR 110. It has a visual magnitude of $9^{\rm m}_{.}06$ and has a spectral type of either B3III (Houk & Smith-Moore 1988) or B1.5V (Hiltner 1956). This star was observed from June 14, 2007 to July 16, 2007 for a little more than 30 days.

Strømgren photometry is available (Hauck & Mermilliod 1998): $H\beta = 2.614$, $b - y = 0.188$, $m1 = 0.011$, $c1 = 0.234$ yielding $T_{\rm eff} = 19071\,{\rm K}$ and $\log g = 3.31 \pm 0.14$ using the calibration method from Napiwotzki et al. (1993) or $T_{\rm eff} = 21102\,{\rm K}$ and $\log g = 4.06$ using the Strømgren calibration by Castelli (1991). While the first calibration puts the star well outside the SPB instability range, the latter puts it within it (see Fig.6.1).

frequency [c/d]	amp [mmag]	sig	S/N
1.105 ± 0.001	3.48	833.91	49.45
1.144 ± 0.001	2.60	604.66	42.10
2.036 ± 0.002	1.68	330.61	31.13
0.165 ± 0.002	1.32	240.62	26.56
1.936 ± 0.002	1.39	221.45	25.48
1.713 ± 0.003	0.85	170.96	22.39
1.747 ± 0.003	1.00	131.79	19.66
1.907 ± 0.003	1.07	123.67	19.04
1.834 ± 0.003	0.86	131.73	19.65
0.126 ± 0.004	0.67	82.20	15.52
3.318 ± 0.004	0.67	75.05	14.83
1.646 ± 0.004	0.62	64.61	13.76
1.086 ± 0.004	0.63	58.18	13.06
0.356 ± 0.005	0.69	53.68	12.55
1.866 ± 0.005	0.68	50.60	12.18
1.774 ± 0.004	0.66	58.45	13.09
4.444 ± 0.005	0.65	48.58	11.93
2.249 ± 0.005	0.49	44.53	11.43
1.807 ± 0.005	0.54	44.78	11.46
3.850 ± 0.005	0.37	37.61	10.50
0.384 ± 0.006	0.57	34.18	10.01
0.210 ± 0.005	0.61	40.53	10.90
0.771 ± 0.006	0.44	31.45	9.60
3.668 ± 0.006	0.48	30.04	9.38
3.907 ± 0.006	0.43	30.00	9.38
1.559 ± 0.006	0.46	27.59	8.99
3.161 ± 0.007	0.38	23.29	8.26
0.630 ± 0.007	0.41	23.71	8.34
2.071 ± 0.007	0.31	22.19	8.07
1.965 ± 0.007	0.40	21.15	7.88
1.169 ± 0.008	0.29	18.01	7.27
2.942 ± 0.008	0.39	16.92	7.04
3.201 ± 0.008	0.32	16.94	7.05
5.012 ± 0.008	0.28	15.50	6.74
3.755 ± 0.008	0.26	15.57	6.76
2.110 ± 0.009	0.27	15.09	6.65
1.340 ± 0.009	0.34	14.48	6.52
1.448 ± 0.009	0.24	13.74	6.35
3.963 ± 0.009	0.29	13.05	6.18
2.858 ± 0.009	0.24	12.48	6.05
4.677 ± 0.010	0.21	10.48	5.54

Table 6.3: Frequencies of HD 166291 which survive the selection procedure and could be used for stellar modeling.

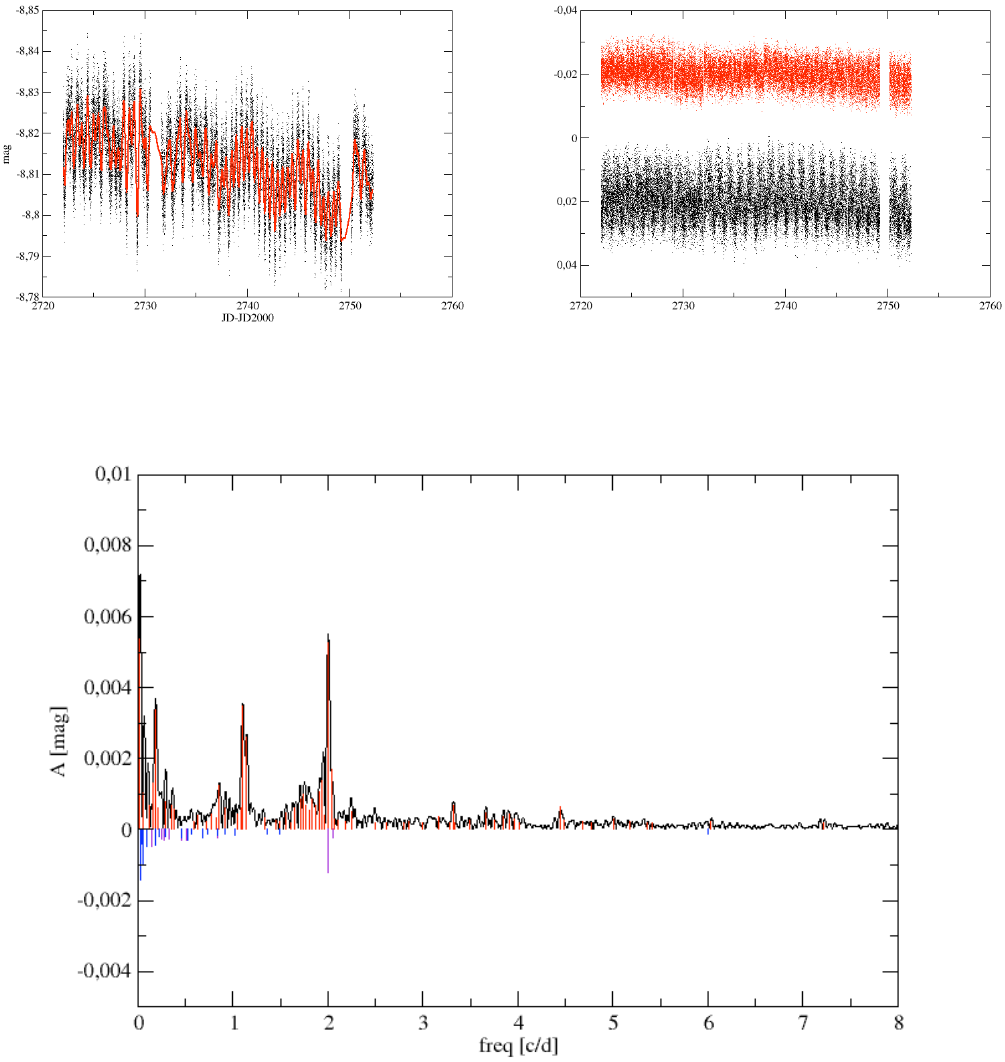

Figure 6.2: Left: Light curve of HD 166291 (black dots) and moving average (red line) observed by MOST. Right: Light curve of the comparison stars HD 165762 (red) and HD 312668 (black). Bottom figure: Amplitude spectrum of HD 166291 with the identified SIGSPEC frequencies in red. The frequencies of the comparison stars are shown in violet (HD 165762) and blue (HD 312668)

6.2 GSC 06265-01026

GSC 06265-01026 (HD 168486) was the 5^{th} guide star in the M17 run. This star has a visual magnitude of $10^{\mathrm{m}}.69$, is classified as B9V star in the SIMBAD astronomical data base and was observed from May 28, 2007 to June 15, 2007 for nearly 18 days.

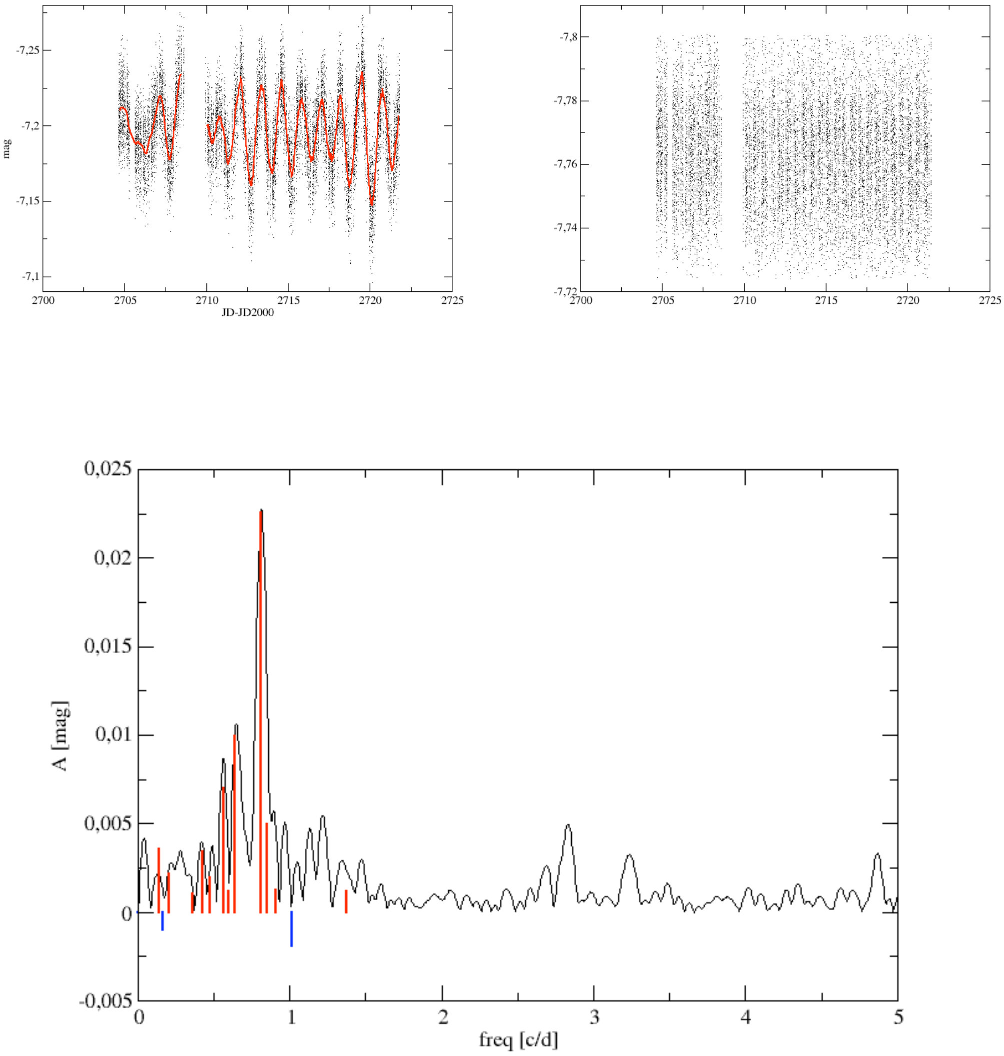

Figure 6.3: Left: Light curve of HD 168486 (black dots) and moving average (red line) monitored for 18 days by MOST. Right: Light curve of the comparison star BD-16 4819. Bottom figure: Amplitude spectrum of HD 168486 with the identified SIGSPEC frequencies in red. The frequencies of the comparison star shown in blue and are directed downwards.

frequency [c/d]	amplitude [mmag]	sig	S/N
0.813± 0.002	22.52	1118.23	57.26
0.636± 0.003	9.92	395.01	34.03
0.567± 0.004	6.99	177.11	22.79
0.853± 0.005	4.99	138.94	20.18
0.427± 0.008	3.42	48.92	11.98
0.138± 0.009	3.54	40.40	10.88
0.907± 0.010	3.21	32.64	9.78
0.202± 0.011	2.14	24.16	8.42
0.698± 0.013	2.74	19.09	7.48
0.746± 0.013	2.05	17.69	7.20
0.472± 0.015	1.96	13.09	6.20
0.597± 0.020	1.18	8.04	4.86
1.375± 0.020	1.19	7.76	4.77
0.363± 0.022	1.06	6.14	4.24

Table 6.4: Frequencies of HD 168486 which survive the selection procedure and could be used for stellar modeling.

6.3 GSC 00154-02450

GSC 00154-02450 (HD 259634), the 34$^{\mathrm{th}}$ guide star in the NGC 2244 run, is identified to star #3005 in the young open cluster NGC 2244 and is a member with a probability of 82% (Chen et al. 2007). The star has a visual magnitude of $9^{\mathrm{m}}.9$ and is classified as a B9III star in the SIMBAD astronomical data base.

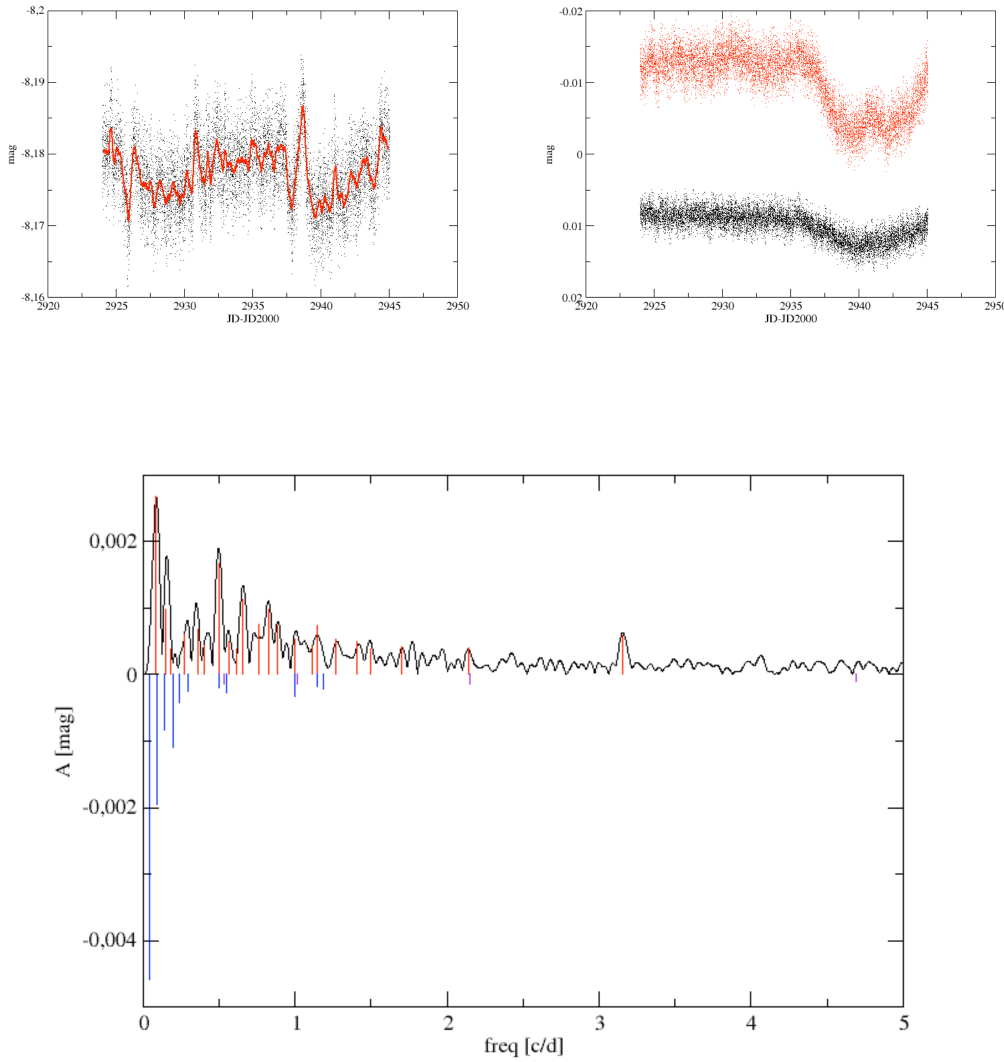

Figure 6.4: Left: Light curve of HD 259634 monitored for 21 days by MOST . In red a running average is shown. Right: Light curve of the comparison stars GSC 00154-01521(HD 46202) and in red the light curve of GSC 00154-02077 (HD 259480) as already shown in chapter 5.1. The Bottom figure shows the amplitude spectrum with the identified frequencies of HD 259634 in red and the frequencies of the comparison star in blue.

frequency [c/d]	amplitude [mmag]	sig	S/N
0.658± 0.005	1.17	91.67	16.39
0.825± 0.006	0.98	63.16	13.61
0.351± 0.008	0.75	36.85	10.39
0.760± 0.008	0.75	33.56	9.92
0.883± 0.008	0.72	35.19	10.16
1.140± 0.009	0.74	29.39	9.28
3.158± 0.009	0.59	28.85	9.20
1.270± 0.010	0.54	24.12	8.41
0.265± 0.010	0.54	21.67	7.97
1.409± 0.010	0.50	21.18	7.88
0.392± 0.011	0.52	19.99	7.65
1.699± 0.013	0.42	13.67	6.33
1.109± 0.014	0.43	11.88	5.90
1.499± 0.014	0.39	12.39	6.03
0.456± 0.013	0.41	12.51	6.05
0.618± 0.015	0.39	10.73	5.61

Table 6.5: Frequencies of HD 259563 which survive the selection procedure and could be used for stellar modeling.

6.4 GSC 00158-03064

GSC 00158-03064 (HD 259440) was the 1st guide star in the HD 46375 run. This star has a visual magnitude of $9\overset{m}{.}12$ and is classified as B0pe star in the "Catalog of Hα emission stars in the northern Milky Way" by (Kohoutek & Wehmeyer 1999). This should indicate a SPBe star, as it did in Section 5.1. This star was observed from December 14, 2005 to January 26, 2006 for nearly 41 days.

Strømgren photometry including a $H\beta$ measurment is available both by Hauck & Mermilliod (1998) and Kilkenny et al. (1985) providing the following values: $H\beta = 2.420$, $b{-}y = 0.476$, $m1 = -0.113$, $c1 = 1.694$. Independent on the calibration method used, these values do not deliver physical values for neither $\log g$ nor T_{eff}. The software tools used to calibrate the Strømgren values indicate that $c1$ is out of range, i.e. yielding an unrealistic value.

One can clearly see the frequency groupings of a SPBe star in the amplitude spectrum (see Section 5.1.2).

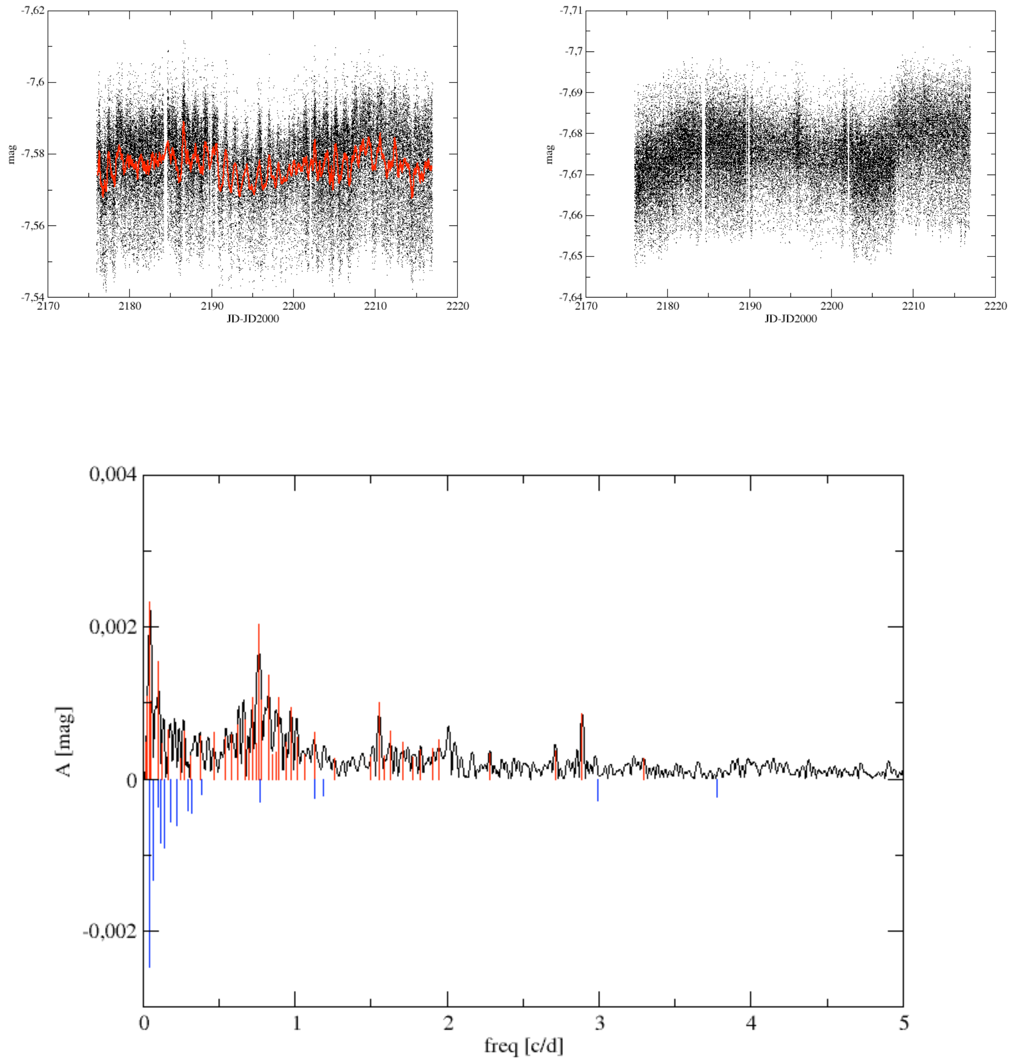

Figure 6.5: Left: Light curve of HD 259440 (black dots) including a moving average (red line) monitored for 41 days by Most. Right: Light curve of the comparison star HD 258721. Bottom figure: Amplitude spectrum of HD 259440 with the identified SigSpec frequencies in red. The frequencies of the comparison star shown in blue and are directed downwards.

frequency [c/d]	amplitude [mmag]	sig	S/N
0.763 ± 0.002	2.04	177.86	22.84
0.097 ± 0.002	1.55	95.79	16.76
0.826 ± 0.003	1.37	95.07	16.69
0.724 ± 0.003	1.07	81.06	15.42
0.781 ± 0.004	1.04	42.63	11.18
0.895 ± 0.003	1.06	52.37	12.39
2.889 ± 0.003	0.86	53.32	12.50
0.626 ± 0.003	0.72	52.14	12.36
0.974 ± 0.004	0.94	48.22	11.89
1.553 ± 0.003	1.00	49.52	12.05
0.670 ± 0.004	0.78	42.21	11.12
0.544 ± 0.004	0.55	29.93	9.37
0.268 ± 0.004	0.63	29.97	9.37
0.165 ± 0.005	0.64	25.70	8.68
0.378 ± 0.005	0.56	23.98	8.38
0.469 ± 0.005	0.61	22.72	8.16
0.943 ± 0.005	0.49	21.02	7.85
1.624 ± 0.006	0.62	16.74	7.00
1.709 ± 0.006	0.49	17.49	7.16
1.946 ± 0.006	0.52	14.94	6.62
0.743 ± 0.007	0.47	13.93	6.39
1.906 ± 0.007	0.39	13.70	6.34
0.583 ± 0.007	0.58	13.59	6.31
2.713 ± 0.007	0.38	10.70	5.60
0.875 ± 0.008	0.36	9.72	5.34
1.827 ± 0.008	0.38	9.16	5.18
0.695 ± 0.009	0.39	8.14	4.89
2.282 ± 0.009	0.34	7.81	4.79
1.776 ± 0.009	0.29	7.22	4.60
1.587 ± 0.009	0.31	6.95	4.51
1.065 ± 0.010	0.31	6.50	4.36
0.849 ± 0.010	0.31	6.10	4.23
0.246 ± 0.010	0.27	5.49	4.01
3.291 ± 0.010	0.27	5.43	3.99

Table 6.6: Frequencies of HD 259440 which survive the selection procedure and could be used for stellar modeling.

6.5 GSC 06276-01284

GSC 06276-01284 (HD 313925) was the 15$^{\mathrm{th}}$ guide star in the WR 110 run. This star has a visual magnitude of $10\overset{\mathrm{m}}{.}6$, is classified as B5 star in the SIMBAD astronomical data base and was observed from June 6, 2006 to June 28, 2006 for nearly 22 days.

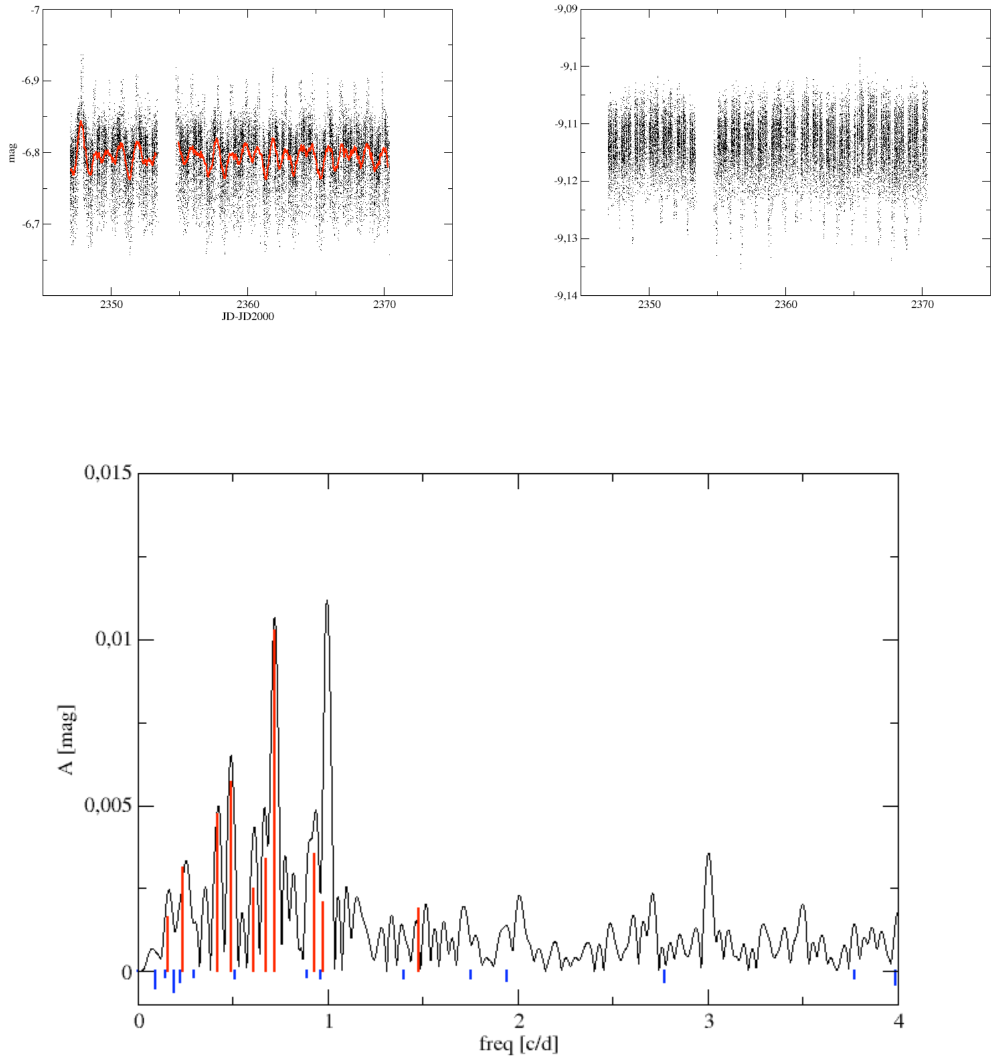

Figure 6.6: Left: Light curve of HD 313925 (black dots) including a moving average (red line) monitored for 22 days by MOST. Right: Light curve of the comparison star HD 166307. Bottom figure: Amplitude spectrum of HD 313925 with the identified SIGSPEC frequencies in red. The frequencies of the comparison star shown in blue and are directed downwards.

frequency [c/d]	amplitude [mmag]	sig	S/N
0.719± 0.003	10.26	243.92	26.74
0.489± 0.005	5.69	77.99	15.12
0.419± 0.006	4.73	60.30	13.30
0.929± 0.007	3.54	41.12	10.98
0.677± 0.009	3.37	24.39	8.46
0.609± 0.012	2.49	15.21	6.68
1.482± 0.016	1.89	7.61	4.72

Table 6.7: Frequencies of HD 313925 which survive the selection procedure and could be used for stellar modeling.

Chapter 7

Conclusions

Out of 23 possible SPB guide stars available for this thesis, 7 were analyzed comprehensively. A frequency analysis indicates SPB type pulsation in all the amplitude spectra. In addition, effective temperature and surface gravity were determined through multicolor photometry (Strømgren and/or Geneva photometry) finding not only the coolest candidate SPB star to date, GSC 00154-00785, but also two candidate SPBe stars (GSC 00154-02436 and GSC 00158-03064). All determined fundamental parameters are listed in table 7.1. The effective temperature and surface gravity used for stellar modelling are plotted in Fig.7.1. However, follow-up observations, especially high resolution spectroscopy, are required to confirm these findings.

Star	T_{eff} [K]	$\log g$	method
GSC 00154-02436	19956 ± 217	4.070 ± 0.150	Geneva
	20626 ± 310	3.850 ± 0.038	Spectroscopy
	19998	3.754	Theory
GSC 00750-01778	16862 ± 311	4.520 ± 0.220	Geneva
	17282 ± 146	4.370 ± 0.090	Strømgren
	16595	4.279	Theory
GSC 00750-01119	16075 ± 138	4.370 ± 0.130	Geneva
	15608	3.870 ± 0.070	Strømgren
GSC 00750-01876	14692 ± 101	4.640 ± 0.110	Geneva
	15462 ± 414	4.450 ± 0.080	Strømgren
GSC 00154-01871	13605 ± 59	3.797 ± 0.012	Spectroscopy
	13614	3.800	Theory
GSC 09007-02387	12515 ± 51	3.680 ± 0.130	Geneva
	12676	3.900	Theory
GSC 00154-00785	12022	4.004	Theory

Table 7.1: Temperatures and surface gravities of category-A stars.

One can compare the equatorial velocity of the category-A stars obtained from the pulsational stability analysis (see table 7.2) with the $v \sin i$ measurements of all confirmed SPB stars found so far (see Fig.7.2). Except for HD 259481, showing an extremely high rotational velocity as expected for a SPBe star, all candidate stars have a rotational velocity which is comparable to that of the confirmed SPB stars. Geneva multicolor photometry of HD 47469 delivers a different surface gravity value than Strømgren photometry. Therefore two values for the rotational velocity are possible (see Section 5.6).

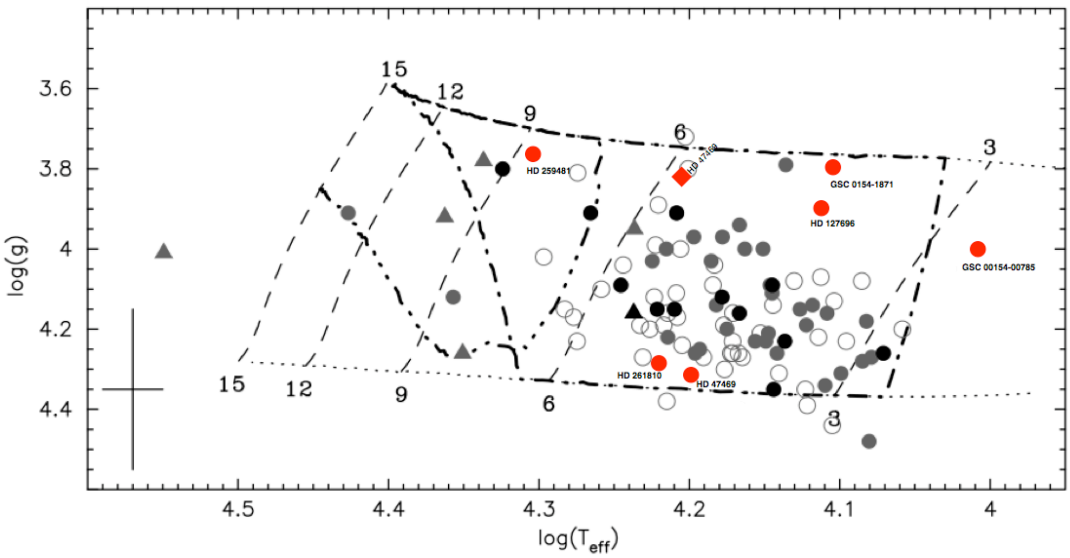

Figure 7.1: Position of confirmed (full symbols), candidate (open symbols) and Most candidate (red circles) SPB stars in the ($\log T_{\rm eff}, \log g$)-diagram. The position of HD 47469 depends on the multicolor photometry used.

Star	velocity [km/s]
GSC 00154-0785	33
HD 127696	80
HD 261810	246
HD 47469	145 / 301
HD 259481	375

Table 7.2: rotational velocity of all category-A stars.

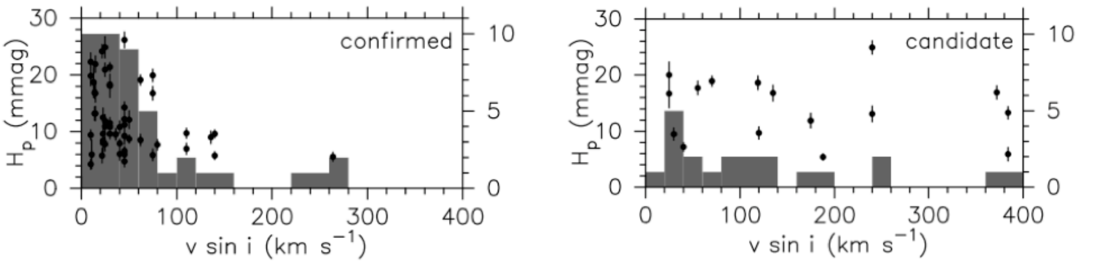

Figure 7.2: Distribution of the projected rotational velocity ($v \sin i$) for the confirmed (left) and candidate (right) SPB stars. (This text and figure was kindly provided by (De Cat 2007))

6 out of the category-A stars are possible members of two young open clusters: GSC 00154-02436 (35%), GSC 00154-00785 (50%) and GSC 00154-01871 (84%) belong to NGC 2244 GSC 00750-01778 (74%), GSC 00750-01876 (94%) and GSC 00750-01119 are possible members of NGC 2264. Since stars of the same cluster have roughly the same distance from Earth and were born at

the same time, consequently the different properties of these stars are simply a function of mass. Therefore clusters are very important if one tries to understand stellar evolution.

The black bars in the histogram in Fig.7.3 show all significant frequencies of all stars, i.e. category-A, B and C. The red bars on the other hand show the frequency distribution excluding (candidate) SPBe stars in this data sample. Comparing this histogram with the histogram of confirmed SPB stars in Fig.2.3 (also shown in the upper right corner of Fig.7.3), one can clearly see a convincing consistency between the two figures. The distribution has its highest peak between 0.6 c/d and 0.7 c/d which is exactly where the highest peak for all confirmed SPB stars lies. Even the gap around 1 c/d can be reproduced. (This occurrence however, is not significant because all frequencies in Fig.2.3 are found via ground-based observations, and therefore the gap has its origins, obviously, in the day-to-night variations. Although Most does not suffer from these variations, it suffers from daily fluctuations of stray-light and the South Atlantic Anomaly (SAA), resulting in corrupt frequencies around 1 c/d which have to be neglected after the frequency analysis). Most of the frequencies in Fig.7.3 lie below 1.5 c/d, which is in agreement with the expected frequency range of theoretically predicted unstable SPB modes (Dziembowski & Pamiatnykh 1993).

As of 2007 (De Cat 2007) 51 confirmed and 65 candidate galactic SPB stars are known. Thanks to Most guide star photometry the sample of SPB stars was increased significantly by at least 9 candidate SPB stars.

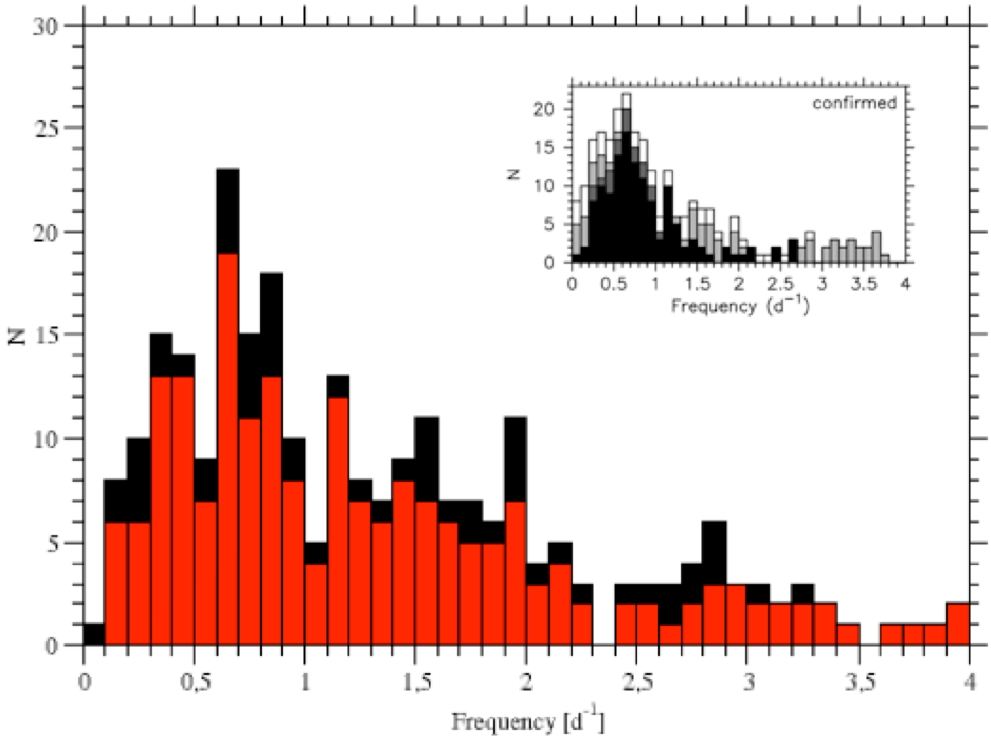

Figure 7.3: The black bars show the number of detected frequencies of all investigated stars in this thesis whereas the red bars exclude stars which are (possible) SPBe stars (e.g. labeled as emission line stars). Upper right corner: Histogram of all confirmed SPB stars (black), MOST observations of HD 163830 (dark grey), HD 163868 (light grey), and HD 163899 (white) known to date (taken from (De Cat 2007))

Acknowledgements

Firstly, I'd like to thank my family, especially my parents for their trust, their financial support and for being there any time I needed them. Without you I definitely wouldn't be where I am today.

I'd also like to thank my supervisor, professor Dr. Werner W. Weiss, for his infinite patience and for always having an open ear for me. I am very grateful that I had the opportunity to be involved in your working group, thus giving me the possibility to get my hands on science so early in my studies.

I don't know how to show my appreciation to professor Dr. Hideyuki Saio. Thank you for your untiring support, your models and help in interpreting the stars. It is because of your assistance that this thesis has scientific value.

I want to thank also Dr. Jaymie Matthews, the father of MOST, for providing me with outstanding data and for many unforgettable nights in Vienna and Vancouver. Cheers!

I'd like to express my deep gratitude to everyone in the "Analysis of Stellar Atmospheres and Pulsation" working group for useful discussion and help in the last three years. Especially Dan, Konstanze, Markus, Michael, Piet, Rainer and Thomas who helped me wherever possible. Thank you guys!

I am also very grateful to you Andrea for your encouragement and consolation in times of negativity and hopelessness. I love you.

Last, but by no means least, I want to thank my best friend Daniel for understanding me even if I say just half a word. Brainlink Bros. Forever.

Bibliography

Aerts, C. 2004, Lecture Notes: Asteroseismology (Lecture Notes: Asteroseimology, by C. Aerts., 2004.)

Aerts, C. & Kolenberg, K. 2005, A&A, 431, 615

Brault, J. W. & White, O. R. 1971, A&A, 13, 169

Breger, M., Stich, J., Garrido, R., et al. 1993, A&A, 271, 482

Briquet, M. & Morel, T. 2007, Communications in Asteroseismology, 150, 183

Burki, G., Grenon, M., Richard, C., et al. 1999

Cameron, C., Saio, H., Kuschnig, R., et al. 2008, ApJ, 685, 489

Castelli, F. 1991, A&A, 251, 106

Chen, L., de Grijs, R., & Zhao, J. L. 2007, AJ, 134, 1368

De Cat, P. 2007, Communications in Asteroseismology, 150, 167

Deeming, T. J. 1975, Ap&SS, 36, 137

Dziembowski, W. A., Moskalik, P., & Pamyatnykh, A. A. 1993, MNRAS, 265, 588

Dziembowski, W. A. & Pamiatnykh, A. A. 1993, MNRAS, 262, 204

Fabry, C. 1927, L'Encyclopedie photometrique (L'Encyclopedie photometrique, vol. 1, ed, by G. Guadet. Paris: Pub. Editions de la Revue d'optique thorique et instrumentale, 1927.)

Gruberbauer, M., Saio, H., Huber, D., et al. 2008, A&A, 480, 223

Hansen, C. J., Kawaler, S. D., & Trimble, V. 2004, Stellar interiors : physical principles, structure, and evolution (Stellar interiors : physical principles, structure, and evolution, 2nd ed., by C.J. Hansen, S.D. Kawaler, and V. Trimble. New York: Springer-Verlag, 2004.)

Hasan, S. S., Zahn, J.-P., & Christensen-Dalsgaard, J. 2005, A&A, 444, L29

Hauck, B. & Mermilliod, M. 1998, A&AS, 129, 431

Hiltner, W. A. 1956, ApJS, 2, 389

Houk, N. & Smith-Moore, M. 1988, in Michigan Spectral Survey, Ann Arbor, Dept. of Astronomy, Univ. Michigan (Vol. 4) (1988), 0–+

Huang, W. & Gies, D. R. 2006, ApJ, 648, 591

Huber, D. 2008, Master thesis: MOST photometry of 10 Aql (Master thesis: MOST photometry of 10 Aql. Vienna:University of Vienna, 2008.)

Huber, D., Saio, H., Gruberbauer, M., et al. 2008, A&A, 483, 239

Hubrig, S., Briquet, M., Schöller, M., et al. 2006, MNRAS, 369, L61

Kallinger, T., Reegen, P., & Weiss, W. W. 2008, A&A, 481, 571

Kharchenko, N. V., Piskunov, A. E., Röser, S., Schilbach, E., & Scholz, R.-D. 2005, A&A, 438, 1163

Kilkenny, D., Whittet, D. C. B., Davies, J. K., et al. 1985, South African Astronomical Observatory Circular, 9, 55

Kippenhahn, R. & Weigert, A. 1990, Stellar Structure and Evolution (Stellar Structure and Evolution, XVI, 468 pp. 192 figs.. Springer-Verlag Berlin Heidelberg New York. Also Astronomy and Astrophysics Library)

Kohoutek, L. & Wehmeyer, R. 1999, A&AS, 134, 255

Kołaczkowski, Z., Pigulski, A., Soszyński, I., et al. 2006, Memorie della Societa Astronomica Italiana, 77, 336

Kunzli, M., North, P., Kurucz, R. L., & Nicolet, B. 1997, A&AS, 122, 51

Lafler, J. & Kinman, T. D. 1965, ApJS, 11, 216

Lee, U. & Baraffe, I. 1995, A&A, 301, 419

Marschall, L. A., van Altena, W. F., & Chiu, L.-T. G. 1982, AJ, 87, 1497

Moffat, A. F. J., Marchenko, S. V., Zhilyaev, B. E., et al. 2008, ApJ, 679, L45

Napiwotzki, R., Schoenberner, D., & Wenske, V. 1993, A&A, 268, 653

Neiner, C., Geers, V. C., Henrichs, H. F., et al. 2003, A&A, 406, 1019

Niemczura, E. 2003, A&A, 404, 689

Ogura, K. & Ishida, K. 1981, PASJ, 33, 149

Pamyatnykh, A. A. 1999, Acta Astronomica, 49, 119

Pena, J. H., Peniche, R., & Cervantes, F. 2000, Contributions of the Observatory of New Mexico State University Las Cruces New Mexico, 401, 1

Reegen, P. 2007, A&A, 467, 1353

Reegen, P., Gruberbauer, M., Schneider, L., & Weiss, W. W. 2008, A&A, 484, 601

Rufener, F. 1976, A&AS, 26, 275

Saio, H., Cameron, C., Kuschnig, R., et al. 2007, ApJ, 654, 544

Shulov, O. S., Kopatskaya, E. N., Khudyakova, T. N., & Khozov, G. V. 1983, Trudy Astronomicheskoj Observatorii Leningrad, 38, 76

Sinachopoulos, D. 1988, A&AS, 76, 189

Turner, D. G. 1976, ApJ, 210, 65

Vasilevskis, S., Sanders, W. L., & Balz, A. G. A. 1965, AJ, 70, 797

Waelkens, C. 1991, A&A, 246, 453

Waelkens, C. & Rufener, F. 1985, A&A, 152, 6

Waelkens, C. L. 1987, Meded. K. Acad. Wet., Lett. Schone Kunsten Belg., Kl. Wet., Vol. 49, No. 1, p. 59 - 92, 49, 59

Walker, G., Matthews, J., Kuschnig, R., et al. 2003, PASP, 115, 1023

Walker, M. F. 1956, ApJS, 2, 365

Curriculum Vitae

David Gruber
Eisvogelgasse 6
1060 Wien
Austria
+43 650 39 59 473
gruber@astro.univie.ac.at

Personal Data

Date & Place of birth: December 6th 1984, Bozen, Italy
Parents: Eduard Gruber and Monika Lafogler *Citizenship*: Italian *Martial status*: single

Education

10/89-07/94
Elementary school "A. Rosmini", Bozen, Italy.

10/94-07/97
Middle school, "A. Stifter", Bozen, Italy.

10/97-06/03
High school, Neusprachliches Lyzeum "Walther von der Vogelweide", Diploma (88/100 points)

10/89-07/94
University of Vienna, Vienna, Austria. BS in Astronomy; Thesis title (under supervision of Prof. Dr. Werner W. Weiss): *Robotic Photometry.*

6/00
High School Diploma; Neusprachliches Lyzeum "Walther von der Vogelweide", Armando Diaz Strasse, Bozen, Italy.

10/03-07/06
University of Vienna, Vienna, Austria. BSc. in Astronomy; Thesis title (under supervision of Prof. Dr. Werner W. Weiss): *Robotic Photometry.*

10/06-01/07
Universitet Uppsala, Uppsala, Sweden (ERASMUS).

02/07-06/09
University of Vienna, Vienna, Austria. MSc. in Astronomy; Thesis title (under supervision of Prof. Dr. Werner W. Weiss): *Slowly Pulsating B Stars Discovered Employing MOST Guide Star Photometry.*

Research Experience

4/05 - Present
Research Student to Dr. Werner W. Weiss; "Asteroseismology along the Main Sequence", Institute of Astronomy, University of Vienna.

7/07
Participant at the conference "Lige International Astrophysical Colloquium, Massive Stars Along The Main Sequence And Close To It", Universit de Lige, Lige, Belgium.

7/07
Participant at the conference "Stellar Pulsation & Cycles of Discovery: New Tools, New Variables, New Astrophysics", University of British Columbia, Vancouver, Canada.

7/07
Participant at the MOST (Microvariability and Oscillation of Stars) Science Team Meeting, University of British Columbia, Vancouver, Canada.

12/05
Participant at the MOST (Microvariability and Oscillation of Stars) Science Team Meeting, Institute of Astronomy, Vienna, Austria.

Work Experience

07/01 - 09/01
Receptionist, Kolpinghaus; Bozen, Italy.

07/02 - 09/02
Receptionist, Kolpinghaus; Bozen, Italy.

07/03 - 09/03
Cleaner, Kolpinghaus; Bozen, Italy.

07/04- 10/04
Cashier, "A22 Brennerautobahn"; Bozen, Italy.

07/05- 10/05
Cashier, "A22 Brennerautobahn"; Bozen, Italy.

07/06- 10/06
Cashier, "A22 Brennerautobahn"; Bozen, Italy.

09/07 - 09/08
Waiter, "blue orange"; Vienna, Austria.

09/07- 11/07

Branch manager, “blue orange”; Vienna, Austria.

Languages

German (first language), Italian, English, French (middle-of-the-road).